

1 Sea-level variability and change along the Norwegian coast between 2 2003 and 2018 from satellite altimetry, tide gauges and hydrography

3 Fabio Mangini¹, Léon Chafik^{2,3}, Antonio Bonaduce¹, Laurent Bertino¹, Jan Even Ø. Nilsen⁴

4 ¹Nansen Environmental and Remote Sensing Center and Bjerknes Centre for Climate Research, Bergen, Norway

5 ²Department of Meteorology and Bolin Centre for Climate Research, Stockholm, Sweden

6 ³National Oceanography Centre, Southampton, UK

7 ⁴Institute of Marine Research and Bjerknes Centre for Climate Research, Bergen, Norway

8 Correspondence to: Fabio Mangini (fabio.mangini@nersc.no)

9 **Abstract.** Sea-level variations in coastal areas can differ significantly from those in the nearby open ocean. Monitoring
10 coastal sea-level variations is therefore crucial to understand how climate variability can affect the densely populated coastal
11 regions of the globe. In this paper, we study the sea-level variability along the coast of Norway by means of in situ records,
12 satellite altimetry data, and a network of eight hydrographic stations over a period spanning 16 years (from 2003 to 2018). At
13 first, we evaluate the performance of the ALES-reprocessed coastal altimetry dataset (1 Hz posting rate) by comparing it
14 with the sea-level anomaly from tide gauges over a range of timescales, which include the long-term trend, the annual cycle
15 and the detrended and deseasoned sea level anomaly. We find that coastal altimetry ~~and outperforms~~ conventional altimetry
16 products ~~at most locations~~ perform similarly along the Norwegian coast. However, the agreement with tide-gauges in terms
17 of trends are on average 10% better when we use the ALES coastal altimetry data. We later take advantage of the coastal
18 altimetry dataset to perform a sea level budget later assess the steric contribution to the sea-level along the Norwegian coast.
19 We find that the thermosteric and the halosteric signals give a comparable contribution to the sea-level trend along the
20 Norwegian coast, except for three, non-adjacent hydrographic stations, where salinity variations affect the sea-level trend
21 more than temperature variations. We also While longer time series are necessary to evaluate the steric contribution to the
22 sea-level trends, we find that the sea-level annual cycle is more affected by variations in temperature than in salinity, and that
23 both temperature and salinity give a comparable contribution to the ~~detrended and deseasoned~~ sea-level change along the
24 entire Norwegian coast. A conclusion from our study is that coastal regions poorly covered by tide gauges can benefit from
25 our satellite-based approach to study and monitor sea-level change.

26 1 Introduction

27 Sea-level is considered a key indicator to monitor the earth's energy imbalance and climate change (e.g., Oppenheimer et al.,
28 2019; von Schuckmann et al., 2018). ~~An accurate estimate of sea level rise is one of the major challenges of climate research~~
29 ~~(e.g., Eyring et al., 2016)~~ An accurate estimate and attribution of sea-level rise at regional scale is one of the major
30 challenges of climate research (Frederikse et al., 2018) with large societal benefit and impact due to the large human

31 population living in coastal areas (e.g., Lichter et al., 2011). The Norwegian coast is no exception. While it appears little
 32 vulnerable to sea-level variations because of its steep topography and rocks resistant to erosion, it has a large number of
 33 coastal cities, most of which have undergone significant urban development in recent times (Simpson et al., 2015).
 34

35 Since August 1992, when NASA and CNES launched the TOPEX/Poseidon mission, satellite altimetry has enormously
 36 expanded our knowledge of the ocean and the climate system (e.g., Cazenave et al., 2018). With the help of satellite
 37 altimetry, oceanographers and climate scientists could observe sea-level variations over almost the entire ocean (e.g., Nerem
 38 et al., 2010; Madsen et al., 2019) and understand their causes (e.g., Richter et al., 2020), detect ocean currents (e.g., Zhang et
 39 al., 2007) and monitor their variability (e.g., Chafik et al., 2015), observe the evolution of climate events (e.g., Ji et al., 2000)
 40 and investigate their origins (e.g., Picaut et al., 2002). Satellite altimetry has made these, and other achievements, possible
 41 because it has provided continuous sea-level observations over large parts of the ocean, in areas where sea-level
 42 measurements were previously only occasional.
 43

44 While invaluable over the open ocean, satellite altimetry measurements have historically been flagged as unreliable in
 45 coastal areas within 20–50 km from the coast (e.g., Benveniste et al., 2020). Indeed, the accuracy of radar altimetry, which is
 46 2–3 cm over the open ocean (e.g., Volkov and Pujol, 2012), deteriorates in coastal regions because of technical issues (e.g.,
 47 Xu et al., 2019). ~~Notably, land contaminates~~ *Notably, large variations in the backscattering of the area illuminated by the*
 48 *radar altimeters (for example, due to the presence of land or to patches of very calm water in sheltered areas;* Gómez-Enri et
 49 al., 2010) *contaminate* the returned echoes of radar altimeters, and the complex topography of continental shelves, together
 50 with the irregular shape of most coastlines, makes geophysical corrections in coastal areas less accurate than in the open
 51 ocean.
 52

53 To increase the accuracy of radar altimetry in coastal regions, Passaro et al. (2014) have developed the Adaptive Leading
 54 Edge Subwaveform (ALES) retracking algorithm. The ALES retracker addresses the altimeter footprint contamination issue
 55 by avoiding echoes from bright targets (e.g., land). Several studies have found a clear improvement of the ALES-reprocessed
 56 satellite altimetry observations over conventional altimetry products in different areas of the World (e.g., Passaro et al.,
 57 2014, 2015, 2016, 2018, 2021), with the new algorithm providing estimates of the altimetry parameters in coastal areas with
 58 levels of accuracy typical of the open ocean (e.g., Passaro et al., 2014).
 59

60 In this paper, we investigate how the ALES-reprocessed satellite altimetry dataset resolves sea-level along the coast of
 61 Norway compared to all the tide-gauge records available over the 16-year period between 2003 and 2018. Indeed, to the best
 62 of our knowledge, previous validation studies have not considered the entire Norwegian coast, but only parts of it: Passaro et
 63 al. (2015) focused on the transition zone between the North Sea and the Baltic Sea, whereas Rose et al. (2019) focused on

64 Honningsvåg, in northern Norway. The Norwegian coast also appears particularly interesting for validation purposes
65 because, during the altimetry period, it is well covered by tide gauges, and because conventional altimetry products have
66 previously failed to reproduce the sea-level trends in the region (Breili et al., 2017). The present study will thus investigate
67 the performance of ALES in relation to these issues.

68
69 We further use the ALES-reprocessed altimetry dataset in combination with a network of hydrographic stations along the
70 coast of Norway to study the local sea-level budget, which is known to be challenging at the regional scale (e.g., Raj et al.,
71 2020; Richter et al., 2012). Richter et al. (2012) have already used tide gauges and hydrographic stations to assess the
72 different contributions to the Norwegian sea-level variability between 1960 and 2010. However, compared to their study, we
73 use the coastal altimetry dataset to reconstruct a monthly mean sea level time series centred over each hydrographic station.
74 This is an advantage over Richter et al. (2012) since ~~the tide gauges and the hydrographic stations can be as far as 100 km~~
75 ~~apart~~ *some of the Norwegian tide gauges are located in sheltered areas and might not be representative of the variability*
76 *captured by the nearest hydrographic station (which can be as far as 100 km apart).* Moreover, compared to Richter et al.
77 (2012), we analyse the annual cycle of the sea-level more in detail by describing how its properties change along the
78 Norwegian coast. *Furthermore, sea-level measurements from satellite altimetry, unlike those from tide gauges, do not need*
79 *to be corrected for vertical land motion.*

80
81 This paper is organized as follows. Section 2 describes the data used in the coastal sea-level signal analysis. An analysis of
82 sea-level components retrieved by each observational instrument is provided in Section 3. The coastal sea level from tide
83 gauges and satellite altimetry are compared in terms of temporal variability and trends in Section 4. Section 5 focuses on the
84 ~~sea-level budget combining~~ *steric contribution to the* sea-level estimates from altimetry, *tide gauges*, and hydrographic data.
85 Section 6 summarizes and concludes.

86

87 **2 Data**

88 **2.1 ALES-reprocessed multi-mission satellite altimetry**

89 To provide more accurate sea-level estimates in coastal regions, the ALES retracker operates in two stages. At first, it fits the
90 leading edge of the waveform to have a rough estimate of the significant wave height (SWH). Then, depending on the SWH,
91 the algorithm selects a portion of the waveform (known as subwaveform) and fits it to estimate the range (the distance
92 between the satellite and the sea surface), the SWH and the backscatter coefficient.

93

94 The dataset is freely available at the Open Altimetry Database website of the Technische Universität München
95 (<https://openadb.dgfi.tum.de/en/>). The European Space Agency (ESA) also provides, through The Sea Level Climate Change

96 Initiative Programme, a coastal satellite altimetry dataset reprocessed with the ALES-retracker. However, it only covers the
97 northern latitudes up to 60°N and, therefore, only part of the region of interest in this study (Benveniste et al., 2020).

98

99 The dataset and includes observations from the following altimetry missions: Envisat (version 3), Jason-1, Jason-1 extended
100 mission, Jason-1 geodetic mission, Jason-2, Jason-2 extended mission, Jason 3, SARAL, SARAL drifting phase, Sentinel 3A
101 and Sentinel 3B. These are provided at a 1 Hz posting rate (equivalent to an along-track resolution of circa 7 km) and cover
102 the period from June 2002 to April 2020, with the exception of one data gap between November 2010 (end of Envisat) and
103 March 2013 (start of SARAL) to the north of 66° N. Data from different missions have been cross-calibrated, so that there
104 are no inter-mission biases.

105

106 Among all the corrections applied to the altimetry data, the geophysical corrections are of particular interest for the purpose
107 of this study. Indeed, to validate the ALES-reprocessed altimetry against the Norwegian tide gauges, the same physical
108 signal must be removed from both datasets. The geophysical corrections applied to the ALES-reprocessed altimetry data
109 include the tidal and the dynamic atmospheric corrections (COSTA user manual,
110 http://epic.awi.de/43972/1/User_Manual_COSTA_v1_0.pdf). The tidal correction is performed using the EOT11a tidal
111 model. The dynamic atmospheric correction (DAC), available at <https://www.aviso.altimetry.fr/index.php?id=1278>,
112 removes both the wind and the pressure contribution to the sea-level variability at timescales shorter than 20 days, and only
113 the pressure contribution to the sea-level variability at longer timescales. The high-frequency component of the DAC is
114 computed using the Mog2D-G High Resolution barotropic model (Carrère and Lyard, 2003), and it is removed because it
115 would otherwise alias the altimetry data. The low-frequency component accounts for the static response of the sea-level to
116 changes in pressure, a phenomenon also known as inverse barometer effect (IBE), and according to which a 1 hPa
117 increase/decrease in sea-level pressure corresponds to a 1 cm decrease/increase in sea-level. This component is computed by
118 Collecte Localisation Satellites (CLS).

119

120 The producers of ALES flag some of the data as unreliable. More precisely, they recommend excluding observations that fall
121 within a distance of 3 km from the coast and whose sea-level anomaly (SLA), SWH, and standard deviation exceed 2.5 m,
122 11 m, and 0.2 m respectively. We have followed these recommendations with one exception: we have lowered the threshold
123 on the sea-level anomaly from 2.5 to 1.5 m because this choice leads to a better agreement between the tide gauges and the
124 ALES altimetry dataset between Måløy and Rørvik, along the west coast of Norway (Fig. 1).

125 2.2 Tide gauges

126 The Norwegian Mapping Authority (Kartverket) provides information on observed water levels at 24 permanent tide gauge
127 stations along the coast of Norway. Data are updated, referenced to a common datum, quality checked, and freely distributed
128 through a dedicated web API (api.sehavniva.no).

129

130 Even though most tide gauges provide a few decades of sea-level measurements, in this study we only consider the period
131 between January 2003 and December 2018 because it overlaps with the time-window spanned by the ALES-altimetry
132 dataset. Moreover, we only select 22 of the 24 permanent tide gauges available: we exclude Mausund, since it has no
133 measurements available before November 2010, and Ny-Ålesund, because it is outside of our region of interest.

134

135 Over the period considered, the only tide gauges with missing values are Heimsjø and Hammerfest, with a 1-month gap, and
136 Oslo, with a 2-month gap. We expect the Norwegian set of tide gauges to map the coastal sea-level with a spatial resolution
137 of circa 130 km as it corresponds to the mean distance between adjacent tide gauges. This estimate should be treated only as
138 a first order approximation of the spatial resolution since the distance between adjacent tide gauges varies along the
139 Norwegian coast and ranges from ~30 km, in southern Norway, to ~300 km, in western Norway (more precisely, between
140 Rørvik and Bodø).

141

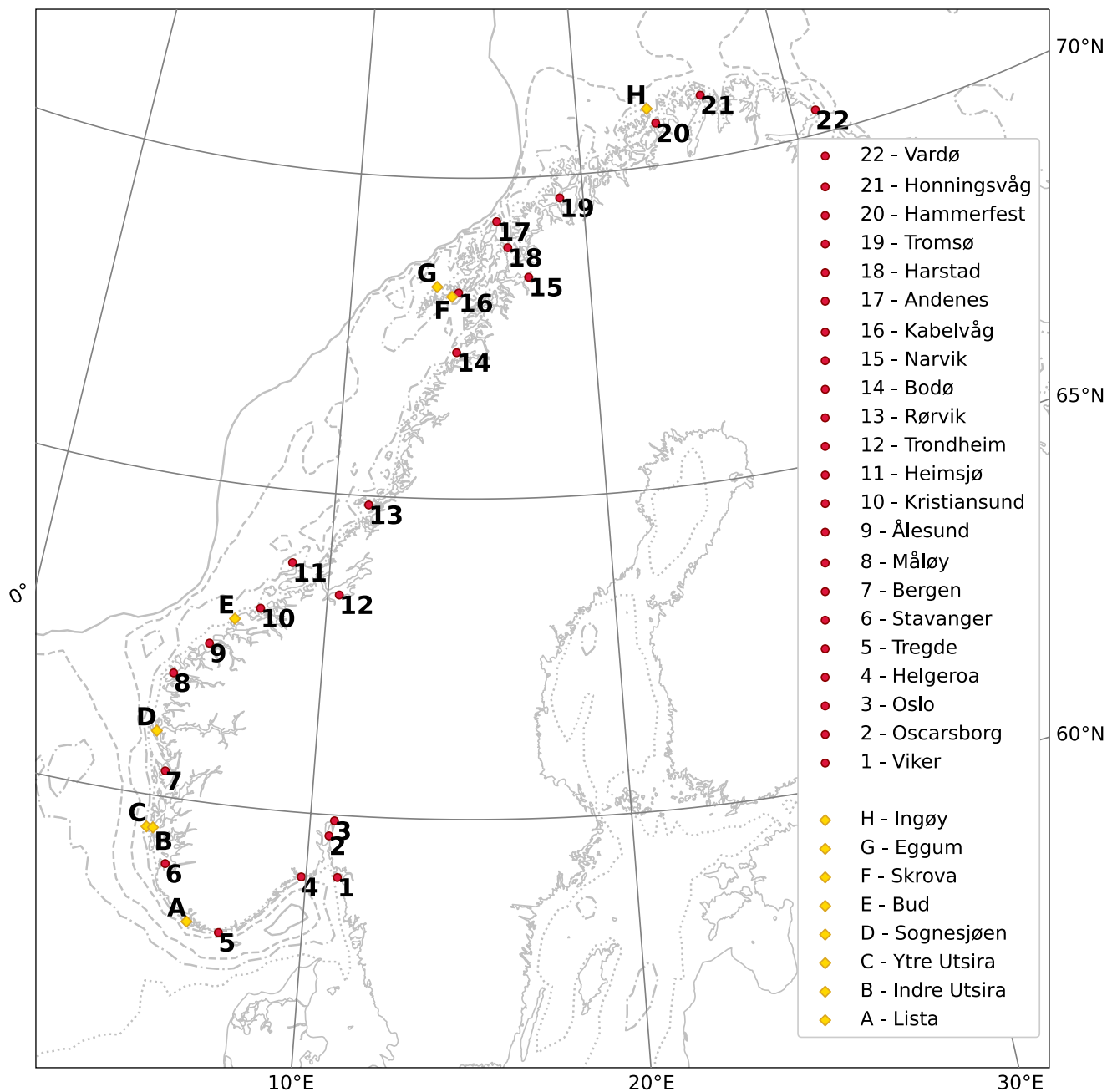


Figure 1: Location of the tide gauges and of the hydrographic stations considered in this study (red circles and yellow diamonds respectively). The solid, dashed, dash-dotted and dotted light gray lines indicate the 500 m, 300 m, 150 m, and 50 m isobaths, respectively.

147 A number of geophysical corrections have been applied to the tide gauge data for them to be consistent with the sea-level
 148 anomaly from altimetry. These include the effects of the glacial isostatic adjustment (GIA), the nodal tide and the DAC.
 149
 150 The GIA results from the adjustment of the earth to the melting of the Fennoscandian ice sheet since the last glacial
 151 maximum, circa 20 thousand years ago. The earth's relaxation affects substantially the sea-level change relative to the
 152 Norwegian coast, with values ranging from approximately 1 up to 5 mm year⁻¹ (e.g., Breili et al., 2017). The GIA affects the
 153 sea-level because it induces a vertical land movement (VLM) and, to a lesser extent, because it modifies the earth's gravity
 154 field. The first effect has been corrected using both GNSS observations and levelling, whereas the second has been corrected
 155 using a GIA model (Simpson et al., 2017).
 156
 157 The low frequency constituents of ocean tide, derived from the EOT11a tidal model, are removed from the tide gauge data as
 158 they are from the ALES-reprocessed altimetry dataset. Hammerfest, Honningsvåg and Vardø, the three northernmost tide
 159 gauges (Fig. 1), are located outside of the EOT11a model domain. Therefore, at these three locations, we remove the low
 160 frequency constituents of ocean tide for Tromsø. The constituents in question are the solar semiannual, solar annual, and the
 161 nodal tide. For Norway the solar annual astronomical tide is negligible, while the two latter constituents have amplitudes on
 162 the order of 1 cm. The nodal tide has a period of approximately 18.61 years and results from the precession of the lunar
 163 nodes around the ecliptic (Woodworth, 2012). As our time series are shorter than the nodal cycle, this constituent is not
 164 negligible with regards to our trend analysis. None of the solid earth related tides needs to be removed from land-locked tide
 165 gauge measurements to produce sea-level records comparable to altimetric sea surface height. Moreover, the ocean pole tide,
 166 not provided by the EOT11a, has not been removed from the tide gauge data. However, it is negligible in our region.
 167
 168 Since we have provided a description of the DAC in the previous section, here we only briefly describe how we have applied
 169 it to the tide gauge data. At first, we have monthly averaged the six hourly DAC dataset (available at the AVISO+ website,
 170 <https://www.aviso.altimetry.fr/en/data/products/auxiliary-products/dynamic-atmospheric-correction.html>). Then, for each
 171 tide gauge, we have computed the difference between the monthly mean sea-level and DAC at the nearest grid point of the
 172 DAC product.

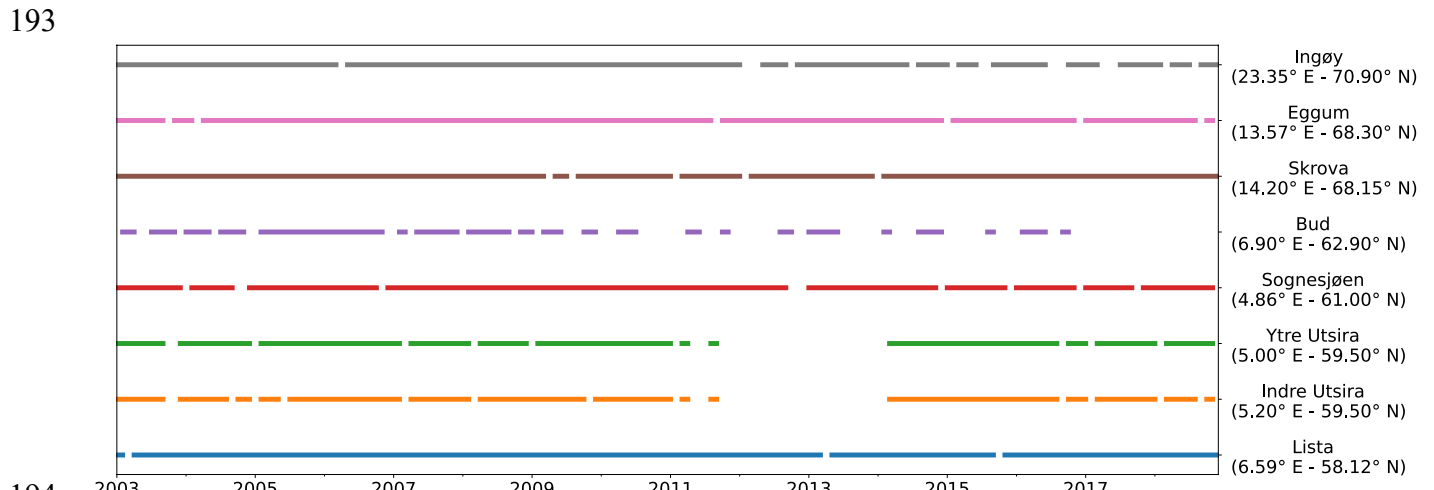
173

174 2.3 Coastal hydrographic stations

175 Over the time window covered by this study, the Institute of Marine Research (IMR) in Bergen, Norway, has maintained
 176 eight permanent hydrographic stations over the Norwegian continental shelf, at a short distance from the coast (Fig. 1). Data
 177 are updated and available at <http://www.imr.no/forskning/forskningsdata/stasjoner/index.html>.

178

179 Along the Norwegian coast, the number of hydrographic stations is approximately one third the number of tide gauges.
 180 Therefore, compared to the tide gauges, the hydrographic stations provide a coarser spatial resolution of the physical
 181 properties of the ocean. We find that the distance between adjacent hydrographic stations is approximately 250 km on
 182 average. This distance is minimum between the twin stations Indre Utsira/Ytre Utsira and Eggum/Skrova, where it does not
 183 exceed 30 km, whereas it is maximum in western Norway, between Bud and Skrova, where it is approximately 670 km.
 184
 185 ~~As for the tide gauges, we~~ We select the temperature and salinity profiles taken between January 2003 and December 2018
 186 for them to overlap with the period covered by the ALES-reprocessed altimetry dataset. The temperature and salinity profiles
 187 at each hydrographic station are irregularly sampled and contain missing values (Fig. 2). Bud has the largest number of
 188 missing values, with 76 gaps out of 192. It is followed by Indre Utsira and Ytre Utsira, with 44 and 41 gaps, respectively.
 189 The remaining hydrographic stations have less than 16 gaps each.
 190
 191 The hydrographic data were used to obtain estimates of the thermosteric and the halosteric sea-level components over the
 192 spatial domain considered in this study.



194
 195 **Figure 2: Data available at each hydrographic station between 01 January 2003 and 31 December 2018.**

196 197 2.4 Atmospheric data

198 To quantify the relationship between the thermosteric component of the sea-level at each hydrographic station and surface
 199 atmospheric temperature, we use the global monthly mean atmospheric temperature at 2 m from the NCEP/NCAR v2
 200 reanalysis dataset (Kalnay et al., 1996) over the period between January 2003 and December 2018. This dataset is provided
 201 on a regular grid with a $2.5^\circ \times 2.5^\circ$ spatial resolution.

203 3 Methods

204 3.1 ~~Sea-level decomposition~~ Harmonic analysis of sea-level

205 Following ~~the~~ a similar approach to the one found in previous papers (e.g., Cipollini et al., 2017; Breili et al., 2017), we use
206 the Levenberg-Marquardt algorithm and fit the following function to sea-level records from remote sensing and in situ data:

$$208 z(t) = a + b \cdot t + c \cdot \sin(2\pi t + d) + e \cdot \sin(4\pi t + f), \quad (1)$$

209 where a is the offset, b the linear trend, c and d the amplitude and the phase of the annual cycle, e and f the amplitude and the
210 phase of the semi-annual cycle. Then, we compare the linear trend, the amplitude and the phase of the annual cycle, and the
211 detrended, deseasoned sea-level signals from remote sensing and in situ data. It is important to note that the use of this
212 formula does not account for interannual variations of the seasonal cycle.

213
214 In the present study, we present the estimates of the sea-level trend from both satellite altimetry and the tide gauges with the
215 corresponding 95% confidence intervals (Fig. 8). Moreover, we assess how strongly the linear trends from altimetry depends
216 on the time period considered and show those trends that are significant at a 0.05 significance level (Fig. 9). To compute the
217 confidence intervals and the statistical significance, we account for the serial correlation in the time series. Indeed,
218 successive values in the sea-level time series might be significantly correlated and, therefore, not drawn from a random
219 sample. To account for this non-zero correlation, we compute the variogram of the detrended and deseasoned SLA from
220 satellite altimetry and the tide gauges and, then, determine the effective number of degrees of freedom, N^* , for each time
221 series (as described in Appendix A).

222
223 We compute the 95% confidence interval of the linear trend as follows:

$$225 CI = t_{0.05/2, N^*-6} \cdot \sqrt{\frac{N-1}{N^*-1}} \cdot SE$$

226 Where SE is the standard error of the linear trend, computed as if $N^* = N$, the total number of observations in the time
227 series, and $t_{0.05/2, N^*-6}$ is the t-value computed using $N^* - 6$ degrees of freedom at a 0.05 significance level.

229 3.2 Colocation of satellite altimetry and tide gauges

230 To compare the sea-level from satellite altimetry and tide gauges, we first need to preprocess the altimetry observations since
231 these are not colocated neither in space nor in time with the tide gauges. The colocation consists of two steps. At first, we

232 select the altimetry observations that are located nearby each tide gauge. Then, we average these observations both in space
 233 and in time to create, for each tide gauge location, a single time series of monthly mean sea-level anomaly from altimetry.
 234

235 During the process, we verify that the selected altimetry observations represent the sea-level variability at each tide gauge
 236 location. More precisely, since tide gauges represent the sea-level variability along a stretch of the coast, the distance from
 237 the coast and along the coast are adjustable parameters of the selection window. At each station, we test different
 238 combinations of the two distances, with the first ranging between 5 and 20 km and the second between 20 and 200 km. Then,
 239 we pick the combination that maximizes the linear correlation coefficient between the detrended and deseasoned SLA
 240 measured by satellite altimetry and by the tide gauge (as, for example, in Cipollini et al., 2017). To select the minimum and
 241 the maximum distances from the coast, we have proceeded as follows. We have set the minimum distance from the coast
 242 following the recommendations on how to use the ALES dataset: these recommend to discard data within 3 km from the
 243 coast. We have then performed a sensitivity analysis and found only small differences between the results obtained applying
 244 a maximum distance of either 40 km or 20 km. To only focus on the observations over the continental shelf, we have
 245 selected the range of distances from the coast between 5 and 20 km. Similarly, we have performed a sensitivity test on the
 246 distance from the tide gauge allowing it to range between 15 and 400 km: as before, we have found little difference in the
 247 final results.
 248

249 We choose to maximize the linear correlation coefficient, instead of minimizing the root mean square differences (RMSDs),
 250 since the former appears less sensitive in cases when there are few altimetry observations. There is one exception are three
 251 exceptions: the Stavanger, Trondheim and Bodø tide gauges, where a very stringent collocation accidentally yields a high
 252 correlation. Thus, for Bodø for these three stations, we select the second highest correlation, which corresponds to a distance
 253 from the coast of 20 km and to a distance along the coast of 200 km.
 254

255 The results suggest that the spatial pattern associated with the detrended and deseasoned sea-level anomaly extends over
 256 hundreds of kilometres. Indeed, the maximum values of the linear correlation coefficients occur for distances along the coast
 257 that range between 140 and 200 km, with them being 200 km at 13 out of 22 tide gauges. Moreover, when, for each tide
 258 gauge, we manually set the distance from the coast and along the coast, respectively, to 20 km and 200 km, we find that both
 259 the linear correlation coefficient and the RMSD vary only little: the first changes by less than 5 %, whereas the second by
 260 less than 4.5 %.
 261

262 We use the process described above to build a time series of monthly mean sea-level anomaly from altimetry at each tide
 263 gauge location. The resulting sea-level time series have no missing values between Viker and Bodø. Instead, to the north of

264 Bodø, they have 29 missing values which result from the lack of altimetry observations between November 2010 and March
265 2013.

267 3.3 Colocation of satellite altimetry and hydrographic stations

268 We preprocess the altimetry observations to examine the steric contribution to the sea-level variability budget at each
269 hydrographic station since the two datasets are not colocated neither in space nor in time. More precisely, we select all the
270 altimetry observations located within 20 km from the Norwegian coast and within 200 km from each hydrographic station.
271 Then, for each station, we monthly average the altimetry observations to build a sea-level anomaly time series from
272 altimetry. The results in the previous subsection give confidence that the monthly mean sea-level computed over such a large
273 area is representative of the sea-level variability at each hydrographic station.

275 3.4 Monthly mean thermosteric, halosteric and steric sea-level components

276 To compute the thermosteric and the halosteric components of the sea-level variability at each hydrographic station, we first
277 monthly average the temperature and salinity profiles. Then, at each hydrographic station, we compute the monthly mean
278 thermosteric and the halosteric components of the sea-level as in Richter et al. (2012):

$$280 \eta_t = \int \alpha(T^*, S^*) \cdot (T - T_0) dz, \quad (2)$$

$$281 \eta_s = \int \beta(T^*, S^*) \cdot (S - S_0) dz, \quad (3)$$

282
283 where α and β are the coefficients of thermal expansion and haline contraction, both computed at $T^* = (T + T_0)/2$ and $S^* =$
284 $(S + S_0)/2$. For each hydrographic station, T_0 and S_0 are reference values and represent time-mean temperature and salinity
285 averaged over the entire water column (Siegismund et al., 2007).

286
287 The steric component of the sea-level at each hydrographic station, η_{st} , is simply the sum of the corresponding thermosteric
288 and halosteric components of the sea-level (Gill and Niller, 1973).

290 3.5 Steric contribution to the Norwegian sea-level

291 At each hydrographic station, we assess the contribution of temperature and salinity to the linear trend and the seasonal cycle
292 of the SLA, and to the detrended and deseasoned SLA.

293

We use simple linear regression to estimate the linear trend of the SLA and of the thermosteric, halosteric and steric components of the sea-level. The seasonal cycle for each time series is considered a monthly climatology. We prefer this procedure over the harmonic analysis approach since the seasonal cycle of the SLA and of the thermosteric, halosteric and steric sea-level depart from the linear combination of the annual and the semi-annual cycles.

4 Comparison of satellite altimetry and tide gauges measurements

In this Section, we assess the quality of the ALES reprocessed coastal altimetry dataset against tide-gauge records by comparing the detrended and deseasoned sea-level variability, the sea-level annual cycle and sea-level trends provided by the remote-sensing and in situ data. We also focus on the stability of linear trend estimates obtained from satellite altimetry (Liebmann et al., 2010; Bonaduce et al., 2016).

4.1 Detrended and deseasoned coastal sea-level

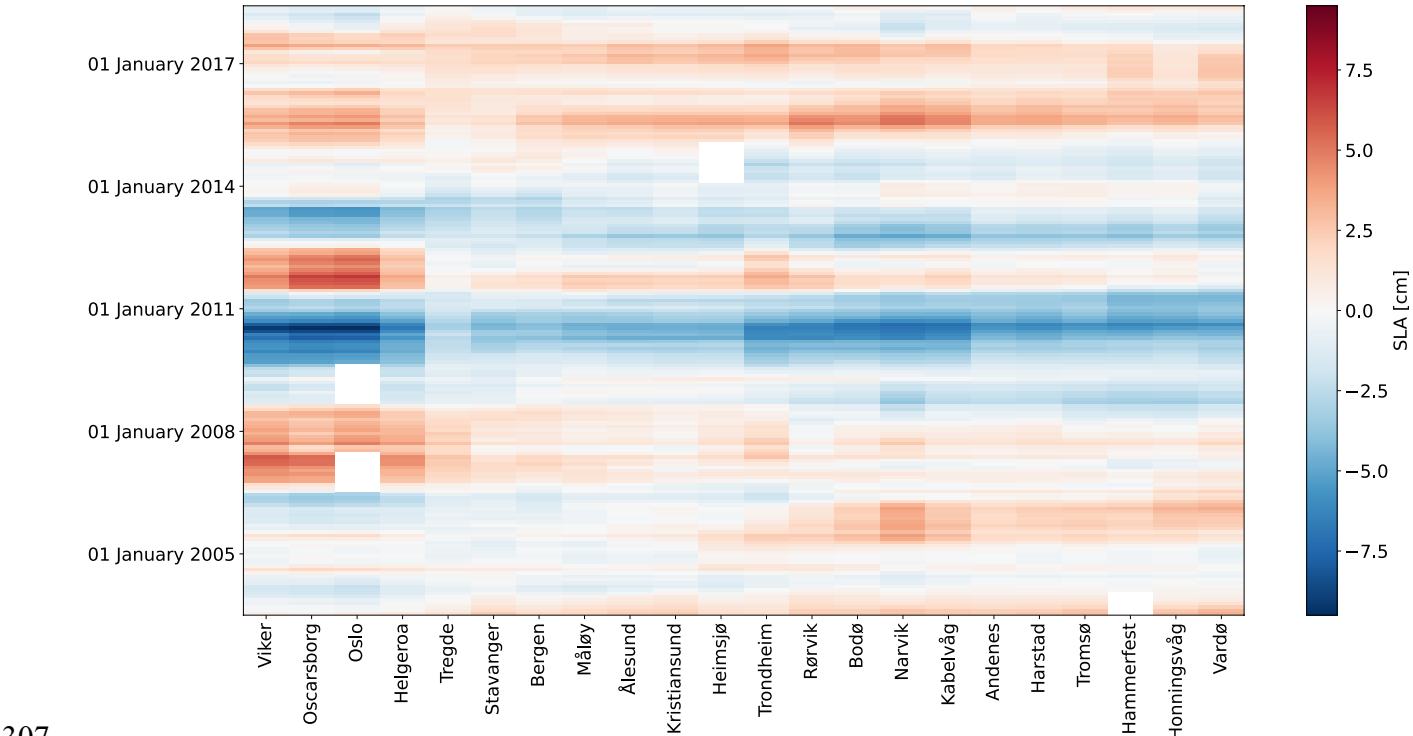


Figure 3: Hovmöller diagram of the detrended and deseasoned monthly mean SLA from tide gauges. The SLA at each tide gauge has been low-pass filtered with a one-year running mean. The tide gauges are displayed on the x-axis. Time is displayed on the y-axis and increases from bottom to top.

311
312
313 Before comparing the detrended and deseasoned SLA from altimetry and tide gauges, we briefly describe how the detrended
314 and deseasoned SLA evolves along the Norwegian coast during the period under study. More precisely, we low-pass filter
315 the detrended and deseasoned SLAs with a one-year running mean to identify their main features at each tide gauge location.
316 Figure 3 shows years when the detrended and deseasoned SLA variations are coherent along the whole Norwegian coast, and
317 years when the sea-level variability occurs at smaller spatial scales (between 100 and 1000 km). As an example, between
318 mid-2009 and the beginning of 2011 circa, the detrended and deseasoned SLA shows negative values of up to -6 cm along
319 the entire Norwegian coast. On the contrary, between 2003 and mid-2009, we note a dipole pattern, with SLA with opposite
320 sign in the south and in the north of Norway. Indeed, up to the beginning of 2006 circa, the Norwegian coast has experienced
321 negative SLA values to the south of Hemsjø and positive SLA to the north of Heimsjø. Over the following three years, the
322 opposite situation has occurred. These results suggest that, although coherent sea-level variability occurs along the
323 Norwegian coast as seen from tide gauges, there are periods when it does not: during these periods, the sea-level variability
324 is likely driven by local changes.
325

1 - Vikør	4 - Helgeroa	7 - Bergen	10 - Kristiansund	13 - Rørvik	16 - Kabelvåg	19 - Tromsø	21 - Honningsvåg
2 - Oscarsborg	5 - Tregde	8 - Måløy	11 - Heimsjø	14 - Bodø	17 - Andenes	20 - Hammerfest	22 - Vardø
3 - Oslo	6 - Stavanger	9 - Ålesund	12 - Trondheim	15 - Narvik	18 - Harstad		

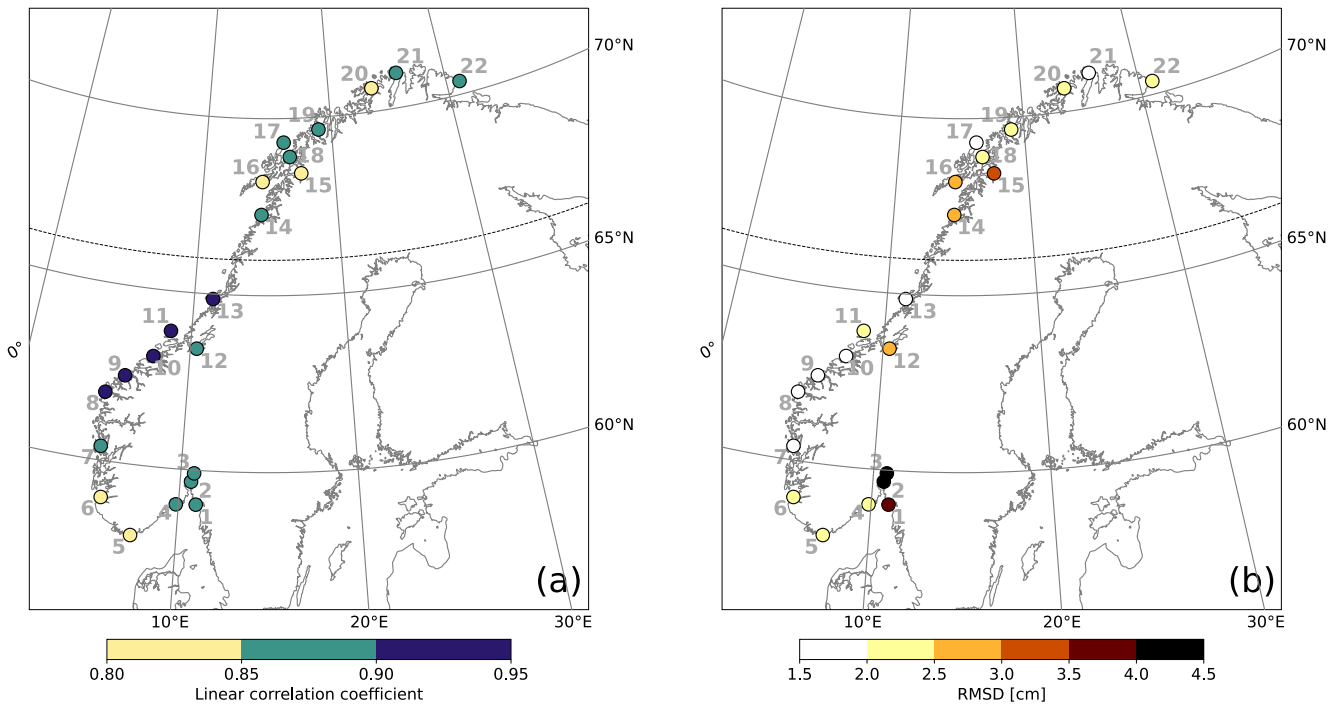


Figure 4: Comparison between coastal sea-level signals from in situ measurements and area-averaged remote-sensing data. At each tide gauge location, linear correlation coefficient (a) and RMSD (b) between the detrended and deseasoned monthly mean SLA from ALES altimetry dataset and from the tide gauge. The black, dashed line indicates the 66° N parallel.

Figure 4 shows a very good agreement between the detrended and deseasoned monthly mean SLA from ALES and the tide gauges. The two datasets agree best along the west coast of Norway where, if we exclude Trondheim, the linear correlation coefficients exceed 0.90 and the RMSDs range between 1.5 and 2.5 cm. As expected, satellite altimetry might performs better between Måløy and Rørvik than in southern and northern Norway because of the convergence of altimeter tracks in the region. We suspect that Trondheim might be is an exception because it is located in the Trondheim fjord, where satellite altimetry might not adequately capture local sea-level variations: the presence of land and patches of calm water affects the quality of the satellite altimetry measurements (Gómez-Enri et al., 2010; Abulaitjiang et al., 2015), and where the complex bathymetry and coastline might lead to imprecise hamper geophysical corrections (Cipollini et al., 2010). Similar peculiarities of the coastline issues might also occur along the Norwegian Trench, in the Skagerrak and in the Oslo fjord, are also likely to affect the agreement, causing where the linear correlation coefficients to fall between 0.80 and 0.90 and the highest RMSDs range between 2.5 and 4.5 cm. Instead, in northern Norway, where we find linear correlation coefficients between 0.80 and 0.90 (statistically significant at a 0.05 significance level) and RMSDs between 1.5 and 3 cm, the problem

might result from the smaller number of altimetry observations in the region. Indeed, only the tracks of Envisat, SARAL, SARAL drifting phase, Sentinel 3A and 3B cover the Norwegian coast north of 66° N.

1 - Viker	4 - Helgeroa	7 - Bergen	10 - Kristiansund	13 - Rørvik	16 - Kabelvåg	19 - Tromsø	21 - Honningsvåg
2 - Oscarsborg	5 - Tregde	8 - Måløy	11 - Heimsjø	14 - Bodø	17 - Andenes	20 - Hammerfest	22 - Vardø
3 - Oslo	6 - Stavanger	9 - Ålesund	12 - Trondheim	15 - Narvik	18 - Harstad		

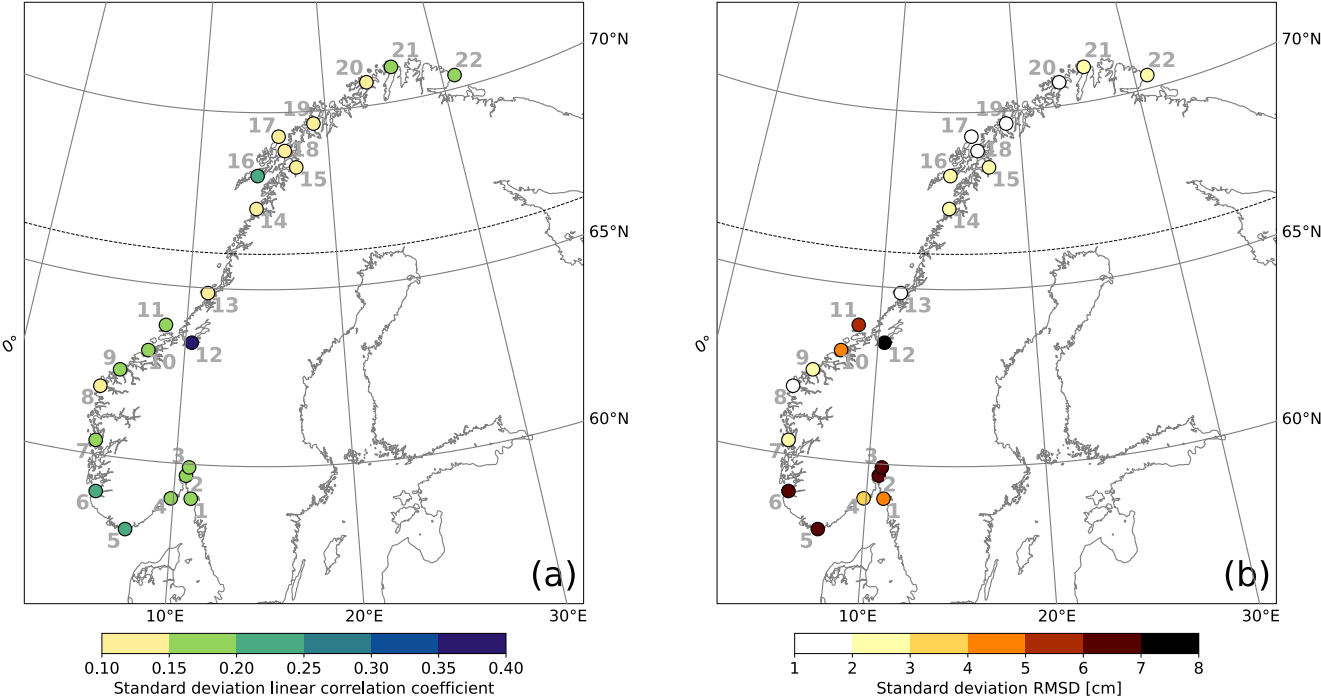


Figure 5: Comparison between coastal sea-level signals from in situ measurements and area-averaged remote-sensing data. At each tide gauge location, standard deviation of the linear correlation coefficients (a) and of the RMSDs (b) computed over each possible combination of the distance from the coast and of the distance from the tide gauge. The black, dashed line indicates the 66° N parallel.

The complex geometry of the Norwegian coast can lead to small-scale variations in sea-level. This can partly explain the difference between the sea-level estimates from tide gauges and from altimetry. Indeed, while the SLA time series measured by the tide gauges are representative for particular locations, those from satellite altimetry, preprocessed as described above, are representative for a spatial domain around the tide-gauge positions. Here, we give an estimate of the geometrical uncertainty on the SLA estimates from satellite altimetry by computing the standard deviation of the linear correlation coefficient and of the RMSD over all the possible combinations of the distance from the coast and of the distance along the coast, as shown in Fig. 5.

These results suggests that the detrended and deseasoned SLA in the south vary over smaller spatial scales compared to the north. Indeed, both the linear correlation coefficient and the RMSD in southern Norway depend more on the size of the selection window than in northern Norway. In Fig. 5a, we note that the standard deviation of the linear correlation coefficients mainly ranges between 0.15 and 0.20 to the south of Trondheim, whereas it ranges between 0.10 and 0.15 to the north of Trondheim. Likewise, the standard deviation of the RMSD follows a similar spatial pattern, with southern Norway showing higher values compared to northern Norway.

4.2 Annual cycle of coastal sea-level

1 - Viker	4 - Helgeroa	7 - Bergen	10 - Kristiansund	13 - Rørvik	16 - Kabelvåg	19 - Tromsø	21 - Honningsvåg
2 - Oscarsborg	5 - Tregde	8 - Måløy	11 - Heimsjø	14 - Bodø	17 - Andenes	20 - Hammerfest	22 - Vardø
3 - Oslo	6 - Stavanger	9 - Ålesund	12 - Trondheim	15 - Narvik	18 - Harstad		

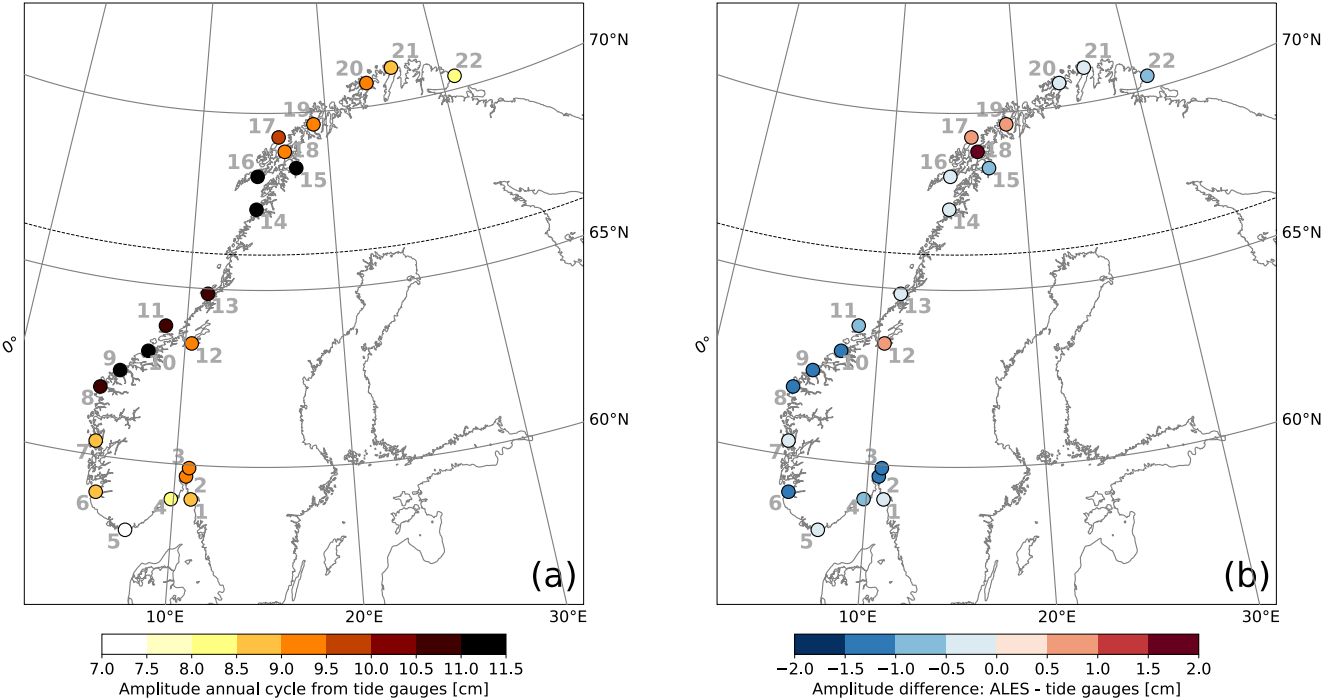


Figure 6: Comparison between the amplitude of coastal sea-level annual cycle from in situ measurements and area-averaged remote-sensing data. At each tide gauge location, amplitude of the annual cycle from the tide gauges (a) and difference between the amplitude of the annual cycle from the ALES-reprocessed altimetry dataset and the tide gauges (b). The black, dashed line indicates the 66° N parallel.

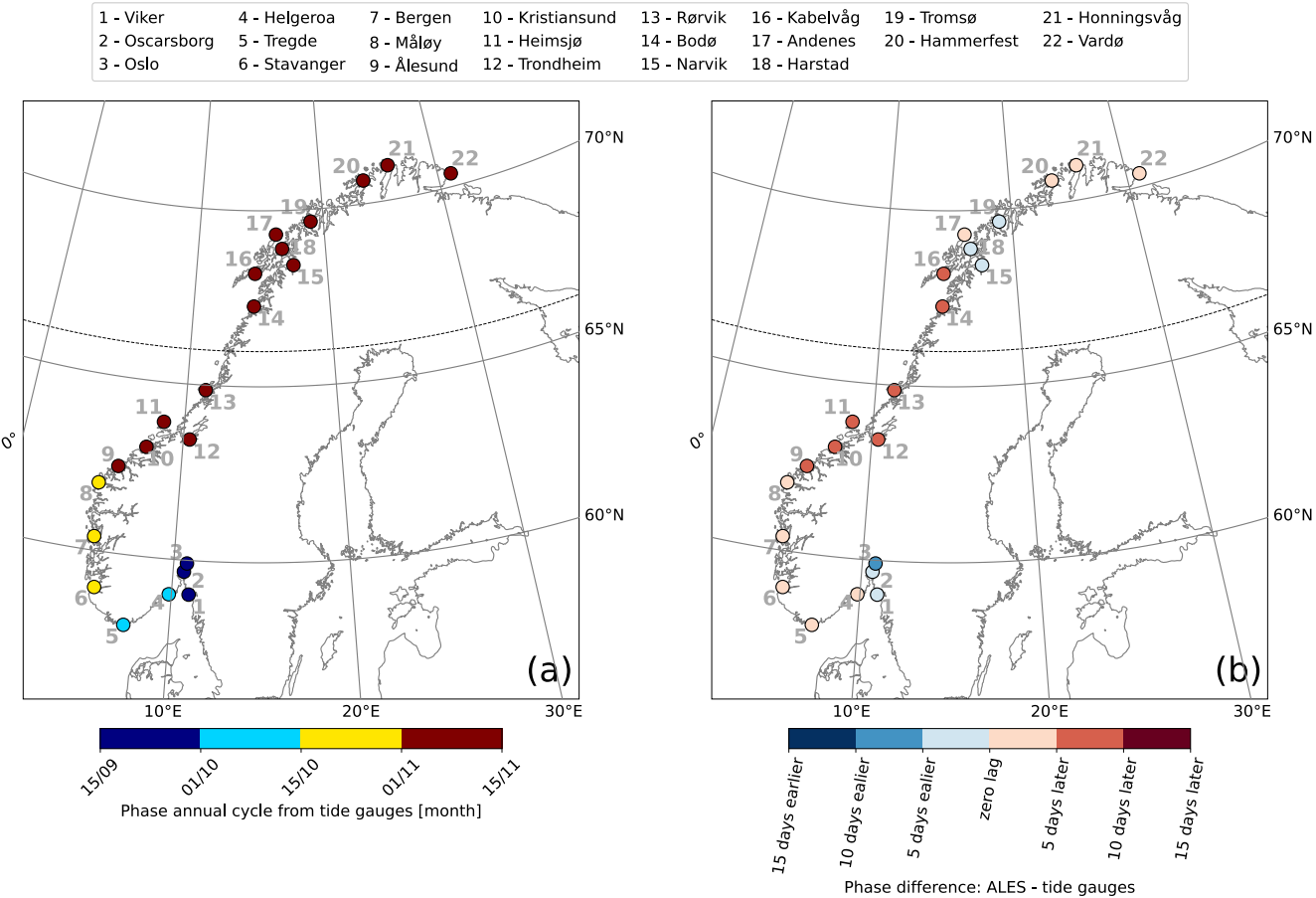
Figures 6 and 7 show a good agreement between the annual cycle estimated using the ALES altimetry dataset and the tide gauges. The difference between the amplitudes of the annual cycle from ALES and the tide gauges ranges between -1.2 and 1.8 cm. However, at most tide gauge locations (16 out of 22), the differences are much smaller, between -1 and 1 cm, less

377 than 10 % of the amplitude of the corresponding annual cycle (Fig. 6a). We note that the differences between the amplitudes
 378 are mostly negative along the southern and western coast of Norway and that, to the north of Rørvik, they become smaller,
 379 and even change sign at some locations (Fig. 6b).

380

381 The difference between the phases of the annual cycle estimated using the ALES altimetry dataset and the tide gauges ranges
 382 between -10 and +10 days (Fig. 7b). Such a great similarity indicates that both radar altimetry and the tide gauges capture the
 383 phase lag of approximately two months between the annual cycle in the north and in the south of Norway. The annual cycle
 384 peaks during the second half of September in the Skagerrak and in the Oslo fjord region, in October along the Norwegian
 385 Trench and in south-west Norway, and mainly during the first week of November north of Kristiansund.

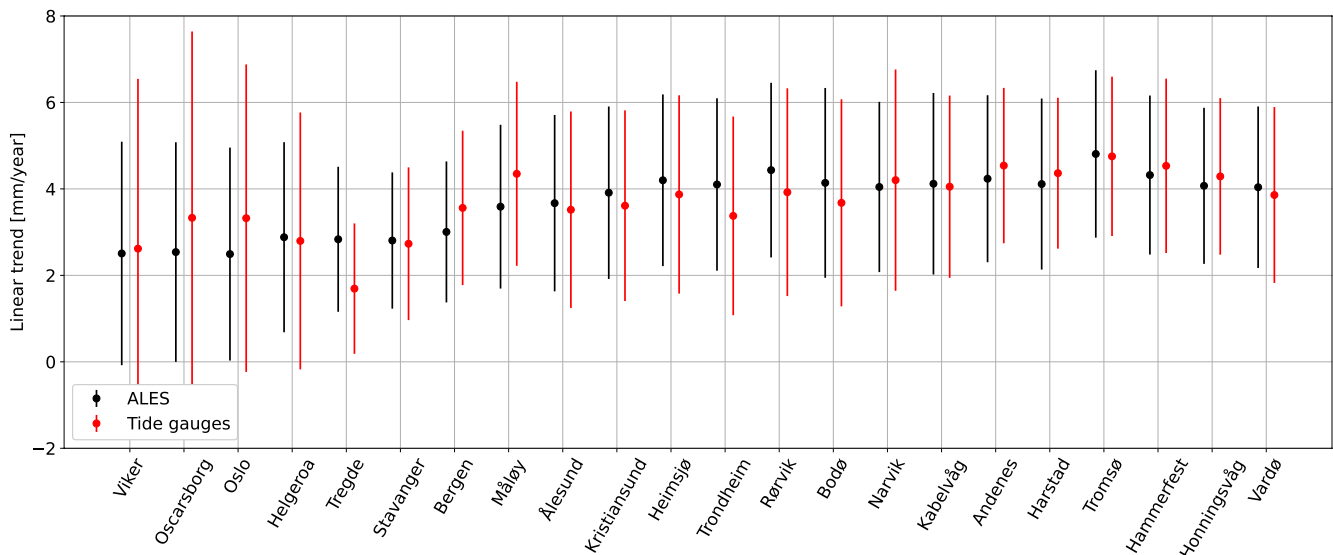
386



387
 388 **Figure 7: Comparison between the phase of coastal sea-level annual cycle from in situ measurements and area-averaged remote-**
 389 **sensing data. At each tide gauge location, phase of the annual cycle from the tide gauges (a) and phase difference of the annual**
 390 **cycle from the ALES-reprocessed altimetry dataset and from the tide gauges (b). The black, dashed line indicates the 66° N**
 391 **parallel.**

392

394 **4.23 Linear trend of coastal sea-level**



395 **Figure 8: At each tide gauge location, linear trend of the SLA from the ALES-reprocessed altimetry dataset (black dots and cyan**
396 **dashes) and from tide gauges (red dots). The cyan dashes indicate the linear trend of the sea-level from ALES when we only**
397 **consider the altimetry observations within 5 km from the coast. The error bars show the 95th confidence intervals of the sea-level**
398 **trend at each tide gauge location.**

401 The differences between sea-level trend estimate obtained from the in-situ and remote-sensed signals range between -0.8 and
402 0.8 mm year^{-1} at most tide gauge stations -0.85 and 1.15 mm/year along the Norwegian coast (Fig. 8). Both datasets return a
403 similar spatial dependence of the sea-level trend along the Norwegian coast, with the lowest values found in the Skagerrak
404 and the Oslo fjord (between 2 and 3 mm year^{-1}), and the highest to the north of Heimsjø (around 4 mm year^{-1}). Moreover, the
405 two datasets return a similar uncertainty of the sea-level trend at each tide gauge location.

406
407 Despite their similarities, we still find that the difference between the sea-level trend from altimetry and tide gauges is
408 statistically significant significantly different from zero at a 0.05 significance level at six 3 out of 22 tide gauges. Following
409 Benveniste et al. (2020), we assess the significance in terms of fractal differences (FD s). Fractal differences are defined as
410 $FD = |\tau| / (1.97 \cdot t_{0.05/2} \cdot SE \cdot \frac{N}{N^*})$, where $|\tau|$ is the absolute value of the linear trend difference between altimetry and each
411 tide gauge, $1.97 \cdot t_{0.05/2}$ is the critical value of the Student t-test distribution for a 95% confidence level with $N^* - 2$ number
412 of degrees of freedom, and SE is the standard error, and N/N^* is the ratio between the total number of observations and the
413 effective number of degrees of freedom. When $FD > 1$, the difference between the two trends is statistically significant at a
414 0.05 significance level, a condition that occurs at Tregde, Måløy, and Bergen Kristiansund, Trondheim, Rørvik and Bodø.

415 Interestingly, ~~only one~~ **none** of these tide gauges is located north of 66° N despite only some of the altimetry missions
416 considered in this study have an inclination exceeding 66° N (namely, Envisat, SARAL, SARAL drifting phase, Sentinel 3A
417 and 3B). Therefore, the fewer altimetry observations to the north of 66° N seem not to deteriorate the agreement between the
418 ALES-reprocessed altimetry and the tide gauges.

419

~~420 We can partly explain the discrepancy between the sea level trend obtained from altimetry and the tide gauges by looking at
421 dependency on the distance from the coast. Indeed, from a visual inspection of Fig. 8, we note that the sea level trend from
422 altimetry and the tide gauges show a better agreement along the south-western coast of Norway, between Kristiansund and
423 Rørvik, when we only consider the altimetry observations within 5 km from the coast. This result is backed by the fractal
424 difference technique, which returns values lower than 1 both at Kristiansund, Trondheim, Rørvik and Bodø.~~

425

426 Following Liebmann et al. (2010), we use the satellite altimetry data to assess how strongly the sea-level trend depends on
427 the time length of the period considered. Each point in Fig. 9 shows the sea-level trend computed over the number of the
428 years on the y-axis, up to the year specified on the x-axis. Between 2003 and 2013 circa, we do not find a significant sea-
429 level trend along the Norwegian coast. Indeed, with very few exceptions, the trends are not statistically different from zero at
430 a 0.05 significance level. The exceptions consist in a small number of cases, each characterized by a sea-level trend lower
431 than -4 mm year^{-1} .

432

433 On the contrary, **with the exception of three southernmost tide gauge locations**, we note a significant positive sea-level trend
434 along the entire coast of Norway when the period considered for the calculation ends in 2015 or later. The linear trends
435 decrease as the length of the period selected increases. When sea-level rates are computed over periods of a few years only,
436 they even exceed 6 mm year^{-1} . Instead, over longer periods of time (e.g., more than 10 years), they mainly range between 3
437 and 5 mm year^{-1} . A visual inspection of the time series confirms that the sea-level has increased since 2014.

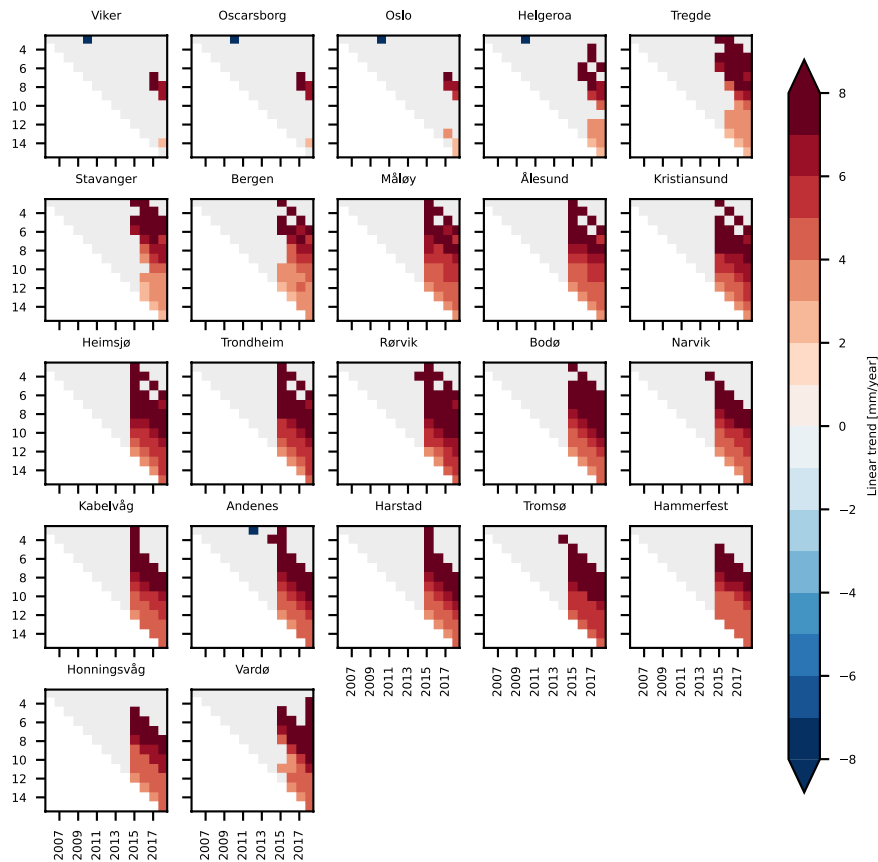


Figure 9: Stability of the sea-level trend along the Norwegian coast. At each tide gauge location, linear trend of the SLA from ALES as a function of the period considered. Each subplot refers to a tide gauge location and shows all the possible trends computed up to the year shown in the x-axis, considering the number of years displayed on the y-axis. For example, the point (x=2014, y=5) in each subplot shows the linear trend of the SLA computed over the 5 years period between 01 January 2009 and 31 December 2014. The light grey colour is used to mask those values that are not significantly different from zero at 0.05 significance level.

5 Sea-level budget Steric contribution to the sea-level variability

In this Section, we use the Norwegian set of hydrographic stations to assess how temperature and salinity affect the sea-level trend, the seasonal cycle of sea-level annual cycle and the detrended, deseasoned sea-level variability at different locations along the Norwegian coast.

452 5.1 Variability of the thermosteric and the halosteric sea-level components

453 The variability of the thermosteric and the halosteric sea-level components along the Norwegian coast mainly occurs over
454 two different spatial and temporal scales (Fig. 10). Notably, the seasonal cycle dominates the thermosteric sea-level
455 variability at each hydrographic station and is responsible for the thermosteric sea-level to vary approximately uniformly
456 along the coast of Norway. On the contrary, the halosteric component shows a variability at shorter spatial- and temporal-
457 scales, possibly due to the contributions from local rivers. The main exceptions are, due to their proximity, the two sets of
458 twin hydrographic stations, Indre Utsira-Ytre Utsira and Eggum-Skrova (Fig. 1).

459
460 Despite these differences, both the thermosteric and the halosteric components of the sea level give a comparable
461 contribution to the sea-level variability along the Norwegian coast (Fig. 10). This ranges approximately between -10 and 10
462 cm at each hydrographic station.

463
464 In the following sections, we investigate the spatial variability of these two components along the Norwegian coast, focusing
465 on the linear trend, the ~~annual~~ seasonal cycle, and the residuals, and on their contribution to the sea-level budget variability
466 in the region.

467

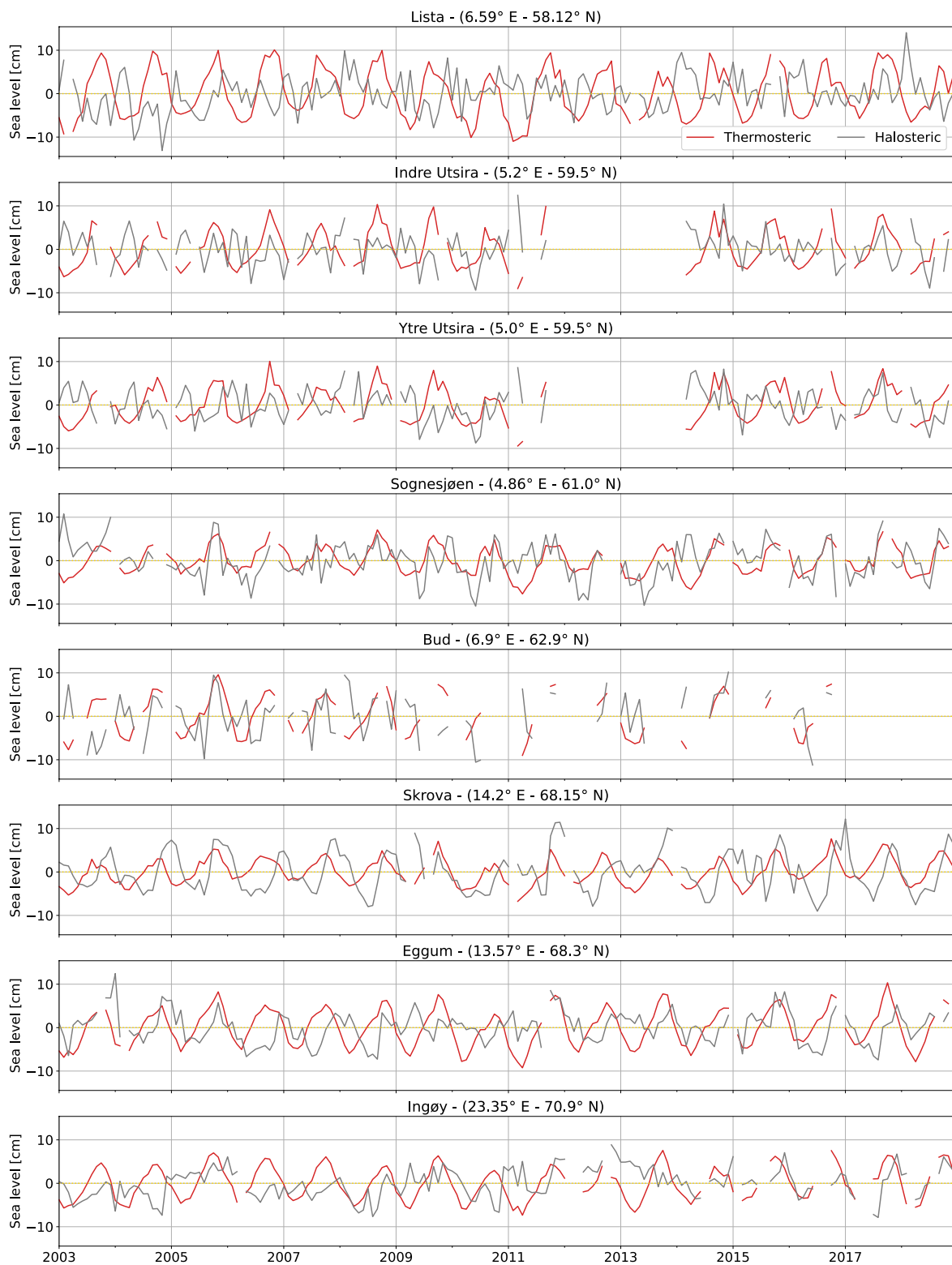


Figure 10: Thermosteric (red) and halosteric (gray) components of the sea-level anomaly at each hydrographic station along the Norwegian coast.

5.2 Linear trend of coastal sea-level and its components Steric contribution to the sea-level trend

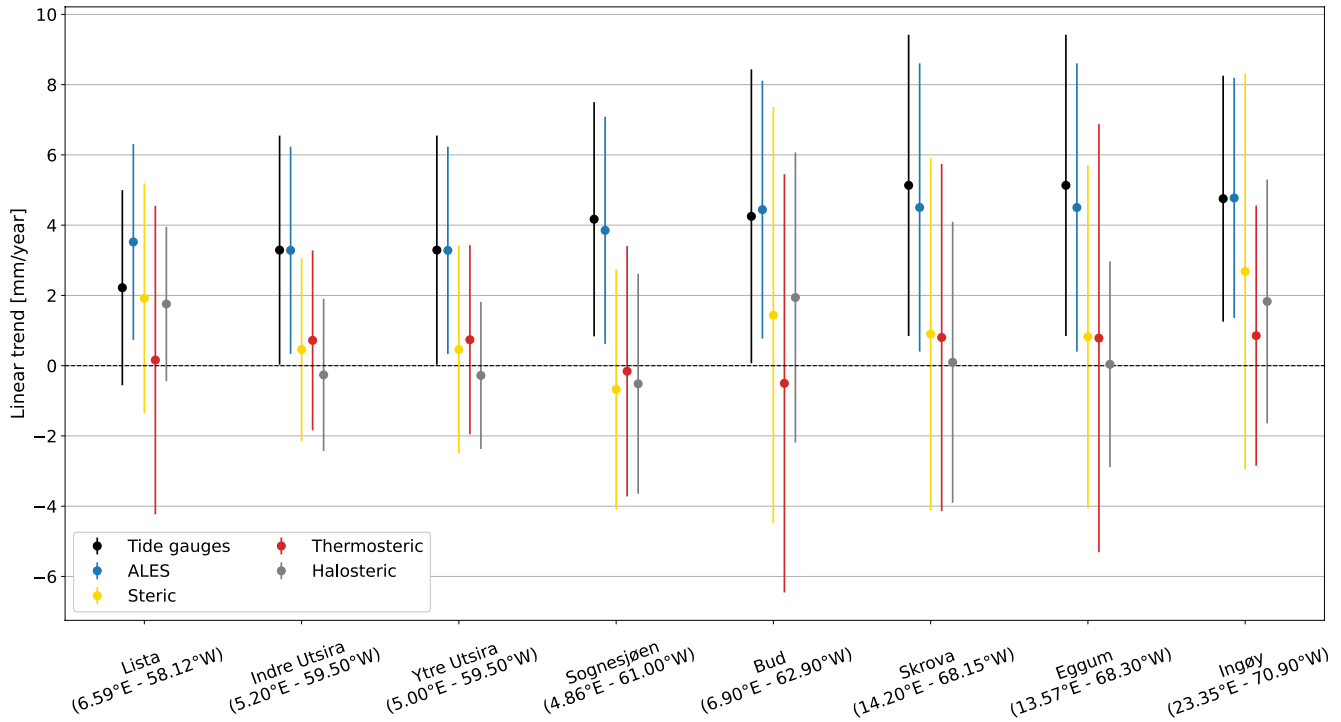


Figure 11: At each hydrographic station, linear trend of the sea-level from tide gauges and from ALES (black and blue dots respectively), and of the steric, thermosteric and halosteric components of the sea-level (green, yellow, red and grey dots respectively). The bars indicate the 95 % confidence intervals.

In this section, we perform a fit-for-purpose assessment of the Norwegian hydrographic station network to obtain estimates of the steric sea-level trends from satellite altimetry and in-situ data.

We find that the linear trends of the thermosteric, halosteric and steric components of the sea-level approximately range between -1.0 and 2.5 mm/year, the width of their confidence intervals ranges between 4.0 and 12.0 mm year⁻¹ circa, with northern Norway exhibiting larger uncertainties (Fig. 11). This is a result of the high inter-annual variability of the thermosteric and the halosteric components in the region (Figs. B1 and B4), which leads to a fewer number of effective degrees of freedom and, therefore, to less accurate estimates of the linear trend.

488 We also test if using tide gauges, instead of satellite altimetry, could alter our estimates of the relative contribution of these
489 components (thermsteric, halosteric and steric) to the sea-level trend along the coast of Norway. Such alteration may indeed
490 occur because the sea-level variations measured by the Norwegian tide gauges might not properly represent those occurring
491 in proximity of the hydrographic stations since the two sets of instruments are not colocated in space (Fig. 1).

492
493 With the exception of Lista, the choice of the dataset has minimal influence on the estimates of the thermsteric, halosteric
494 and steric relative contributions to the sea-level trend along the coast of Norway. We reach this conclusion by visual
495 inspection, but we also provide a more quantitative analysis based on the ratio between the linear-trend of the SLA and of the
496 thermsteric, halosteric and steric components of the sea-level. We find that, apart from Lista, the choice of the dataset
497 modifies such a ratio by less than 13%. At Lista, the change amounts to 59% and results from the ALES-retracked satellite
498 altimetry dataset returning a sea-level trend approximately 1.6 times larger than that provided by the tide gauge at Tregde
499 (this is the tide gauge we use to compute the thermohaline contribution at Lista). Such a large variation is expected since, as
500 we have already noticed, the sea-level rates obtained considering tide gauge and satellite data at Tregde show a less accurate
501 agreement (Figs. 8 and C5).

502
503 ~~In this section, we assess the steric contribution to the sea level trends along the Norwegian coast, considering monthly~~
504 ~~averaged coastal altimetry and hydrographic stations. Figure 11 shows the sea level rates at each hydrographic station~~
505 ~~considered in this study.~~

506
507 ~~Over the period 2003–2018, we observe significant steric contributions to coastal sea level trends, but mostly in the very~~
508 ~~south and the very north of the Norwegian coast, at Lista and Ingøy, with the steric component explaining between~~
509 ~~approximately 40–50 % of the sea level trend estimates obtained from altimetry data. Moreover, when we compare the~~
510 ~~thermsteric and the halosteric signals at these locations, we note that the latter contributes more than the former to the~~
511 ~~coastal sea level trends (up to 60 %).~~

512
513 ~~At the other locations, the steric contribution to coastal sea level is either more uncertain or considerably smaller. At Bud,~~
514 ~~the steric component explains a large fraction of the sea level trend comparable to the one found at Lista and Ingøy, but,~~
515 ~~similarly to Lista and Ingøy, this mainly results from salinity changes. However, the uncertainty associated with these~~
516 ~~estimates are larger at Bud than at the other two stations probably due to the large gaps in the temperature and salinity~~
517 ~~recordings in the second half of the record. At the remaining five locations, the trends induced by the thermsteric, the~~
518 ~~halosteric and the steric sea level are considerably smaller than the altimetry rates. This suggests a larger influence of the~~
519 ~~non-steric (mass induced) sea level trend in these areas.~~

520

We note that the results in Fig. 11 partly differ from those presented by Richter et al. (2012). Indeed, Richter et al. (2012) shows that the thermosteric sea level trend exceeds the halosteric sea level trend at each hydrographic station: while the thermosteric component of the sea level is positive along the entire Norwegian coast and ranges between approximately 0.5 and 1.0 mm year⁻¹, the halosteric component only ranges between -0.3 and 0.3 mm year⁻¹. Between the thermosteric and the halosteric components of the sea level trends, the latter shows the largest difference with Richter et al. (2012). This is more pronounced at Lista and Ingøy where the sea level trend difference exceeds 1.5 mm year⁻¹. We can attribute, however, the differences between Richter et al. (2012) and the present work to the different time periods dealt by the two studies: Richter et al. (2012) focused on the 1960–2010 period, whereas here we focus on the shorter 2003–2018 period.

We can partly explain the temporal and the spatial variations of the linear trend of the thermosteric sea level anomaly by analysing the air temperature variability at 2 m. Indeed, the thermosteric component and the air temperature at the surface strongly correlate at inter-annual and longer timescales: when we low-pass filter them with a 24-month running mean, the linear correlation coefficient between January 1960 and December 2018 ranges between 0.77 and 0.89 at all the hydrographic stations except for Eggum and Ingøy. A closer look at the thermosteric component of the sea level at these two locations shows that the drop in correlation might not have a physical origin since it is most likely due to suspiciously high values of the thermosteric component in the 70s and the 80s. Moreover, we find that, in agreement with the results in Richter et al. (2012) and in Fig. 11, the linear trend of the atmospheric temperature at 2 m between 1960 and 2010 shows positive values, statistically significant at a 0.05 significance level, at all hydrographic stations, whereas such a condition is satisfied only at Skrova, Eggum and Ingøy between 2003 and 2018. So there was less warming in the past 15 years than during the previous four decades.

To better understand what causes the spatial difference of the halosteric sea level trend along the Norwegian coast, we compute the linear trends at each hydrographic station as a function of depth level (Fig. 12). The results suggest that the large halosteric sea level trends at Lista, Bud and Ingøy occur for different reasons. At Lista, the high values result from a freshening in the bottom layer of the water column, below 100 m depth. At Bud, they mainly result from a freshening of the upper layer of the water column, between 20 and 50 m. Instead, at Ingøy, they are mainly caused by a freshening of the entire water column, with it being particularly intense between 50 and 150 m depth, suggesting remote effects rather than the contribution from local rivers.

Figure 12: Linear trend of the thermosteric (red dots) and the halosteric (grey dots) at each depth level of each hydrographic station. The bars indicate the 95 % confidence interval.

555 **5.2 Annual cycle of coastal sea level and its components**

556 We now assess the thermosteric, halosteric, and steric components of the sea-level annual cycle at each hydrographic station
557 along the Norwegian coast.

558

559 Contrary to what we observe for the sea level trends, the steric sea level gives a non-negligible contribution to the sea-level
560 annual cycle along the entire Norwegian coast (Table 1). Indeed, the steric signal explains more than 60 % of the sea-level
561 annual cycle at six out of eight hydrographic stations.

562

563 In Table 1, we note that the annual cycle of steric sea level is largely associated with ocean thermal expansion: except for
564 Skrova, the thermosteric component shows larger amplitudes than the halosteric component along the Norwegian coast. The
565 largest differences are observed at Lista, Indre Utsira and Ytre Utsira where the thermosteric component exceeds the
566 halosteric sea level signal by 3.2, 5.4 and 4.2 times, respectively.

567

568 While the phase of the thermosteric component changes by less than half a month along the entire Norwegian coast, the
569 halosteric component shows a higher variability. In southern Norway, up to Ytre Utsira, the thermosteric and the halosteric
570 sea level components have almost opposite phase: the thermosteric sea level peaks in the second half of October, whereas
571 the halosteric component peaks at the beginning of the year (Table 2). To the north of Ytre Utsira, the lag between the
572 thermosteric and the halosteric components of the sea level decreases since the halosteric annual cycle peaks between
573 October and November at Sognesjøen, and in December from Bud to Ingøy.

574

575 **Table 1: At each hydrographic station, amplitude of the annual cycle of the thermosteric, halosteric and steric components of the**
576 **monthly mean sea level, and amplitude of the annual cycle of the sea level measured from altimetry. The uncertainty indicates the**
577 **95 % confidence interval. Units are cm.**

	Thermosteric	Halosteric	Steric	Total sea level
Lista (6.59° E – 58.12° N)	6.9 ± 0.5	2.2 ± 0.7	5.5 ± 0.9	7.1 ± 0.7
Indre Utsira (5.20° E – 59.50° N)	5.6 ± 0.4	1.0 ± 0.8	4.6 ± 1.0	7.6 ± 0.8
Ytre Utsira (5.00° E – 59.50° N)	4.8 ± 0.4	1.2 ± 0.8	3.7 ± 1.0	7.6 ± 0.8
Sognesjøen	3.9 ± 0.3	2.4 ± 0.8	6.2 ± 0.8	8.6 ± 0.8

(4.86° E – 61.00° N)				
Bud (6.90° E – 62.90° N)	5.8 ± 0.4	2.9 ± 1.2	7.0 ± 1.1	9.6 ± 1.2
Skrova (14.20° E – 68.15° N)	3.4 ± 0.3	4.5 ± 0.6	6.2 ± 0.7	11.1 ± 1.0
Eggum (13.57° E – 68.30° N)	5.4 ± 0.3	2.7 ± 0.6	6.7 ± 0.6	10.9 ± 1.0
Ingøy (23.35° E – 70.90° N)	4.9 ± 0.3	1.7 ± 0.6	5.5 ± 0.7	9.0 ± 0.9

578

579 **Table 2: At each hydrographic station, phase of the annual cycle of the thermosteric, halosteric and steric components of the**
580 **monthly mean sea level, and phase of the annual cycle of the sea level measured from altimetry. The uncertainty indicates the 95**
581 **% confidence interval. Units are months: 0 stands for 01 January, whereas 12 for 31 December.**

	Thermosteric	Halosteric	Steric	Total sea level
Lista (6.59° E – 58.12° N)	8.7 ± 0.1	1.3 ± 0.7	9.2 ± 0.3	9.4 ± 0.2
Indre Utsira (5.20° E – 59.50° N)	8.5 ± 0.1	1.8 ± 1.5	8.6 ± 0.4	9.6 ± 0.2
Ytre Utsira (5.00° E – 59.50° N)	8.9 ± 0.2	2.6 ± 1.3	9.0 ± 0.5	9.6 ± 0.2
Sognesjøen (4.86° E – 61.00° N)	8.9 ± 0.1	9.8 ± 0.6	9.2 ± 0.3	9.6 ± 0.2
Bud (6.90° E – 62.90° N)	8.9 ± 0.1	11.5 ± 0.7	9.7 ± 0.3	9.9 ± 0.2
Skrova	8.6 ± 0.2	11.2 ± 0.3	10.1 ± 0.2	10.2 ± 0.2

(14.20°E – 68.15°N)				
Eggum (13.57°E – 68.30°N)	8.8 ± 0.1	11.3 ± 0.4	9.6 ± 0.2	10.2 ± 0.2
Ingøy (23.35°E – 70.90°N)	8.9 ± 0.1	11.4 ± 0.7	9.3 ± 0.3	10.1 ± 0.2

5.3 Steric contribution to the seasonal cycle of sea-level

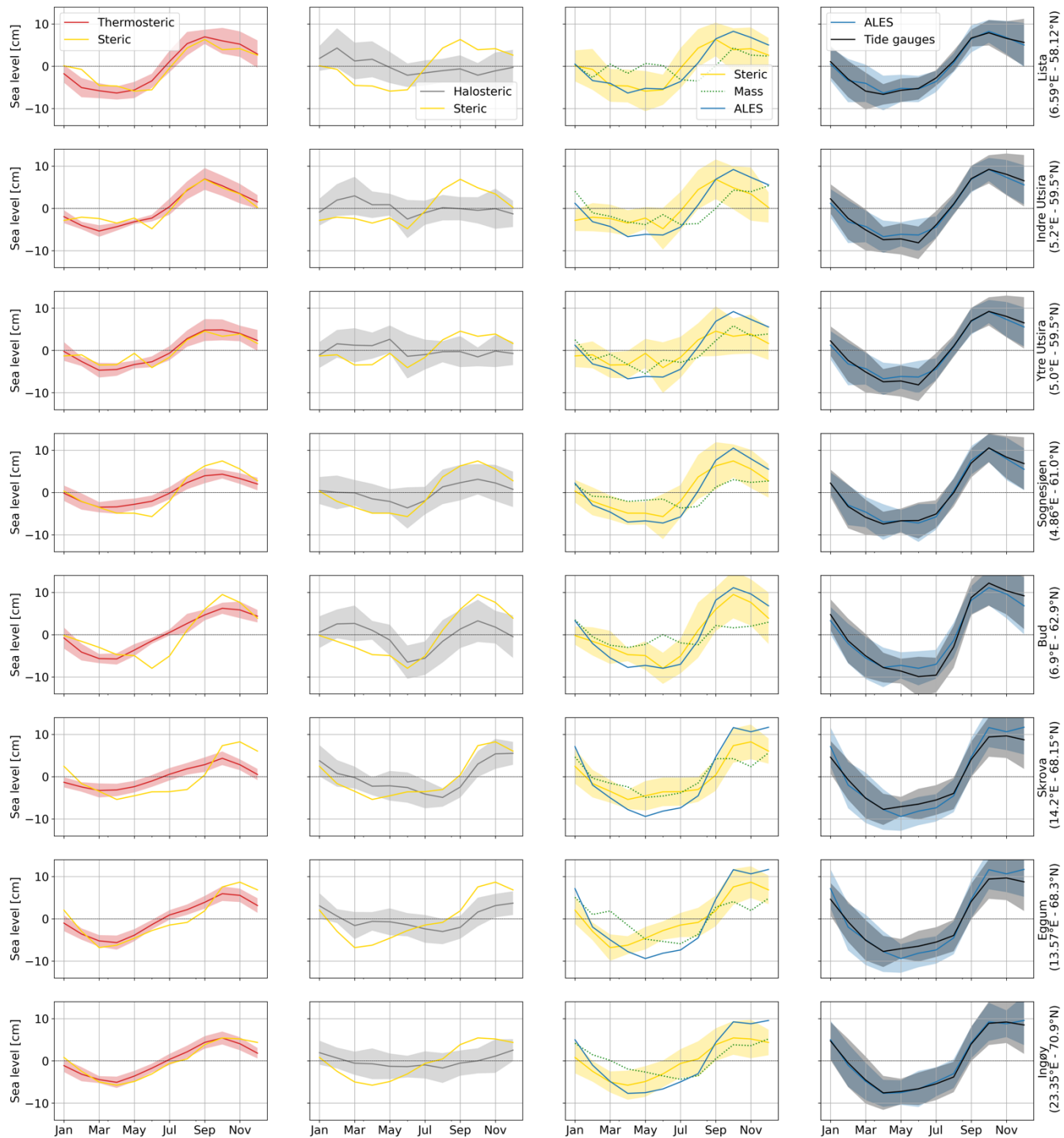


Figure 12: Monthly climatology of the sea-level signals at the hydrographic station positions. The panels show the steric (yellow lines), thermosteric (red lines), halosteric (gray lines), and mass (green lines) components of the sea-level. The monthly climatology

obtained from altimetry (blue lines) and tide-gauge (black lines) measurements are also shown. The shading enveloping the monthly climatologies shows the region departing from each line by one climatological standard deviation.

Table 1: Comparison between the seasonal cycle of SLA from ALES, of SLA from the tide gauges and of steric sea-level at each hydrographic station position. The first and the second columns show, for ALES and the tide gauges, the RMSD between the seasonal cycle of SLA and of the steric sea-level, scaled by the range (maximum minus minimum) of the seasonal cycle of SLA. The third and the fourth columns show the ratio of the amplitudes and the lag of maximum correlation of the seasonal cycle of SLA from ALES and of steric sea-level.

	Scaled $RMSD_{ALES}$	Scaled $RMSD_{Tide\ gauges}$	$\frac{Amplitude_{ALES}}{Amplitude_{Steric}}$	Lag maximum correlation ALES and steric (months)
Lista (6.59°E - 58.12°N)	16%	15%	0.8	1
Indre Utsira (5.20°E - 59.50°N)	21%	23%	0.7	1
Ytre Utsira (5.00°E - 59.50°N)	21%	22%	0.6	1
Sognesjøen (4.86°E - 61.00°N)	13%	14%	0.8	0
Bud (6.90°E - 62.90°N)	12%	16%	0.9	0
Skrova (14.20°E - 68.15°N)	18%	16%	0.7	0
Eggum (13.57°E - 68.30°N)	19%	14%	0.7	0
Ingøy (23.35°E - 70.90°N)	19%	19%	0.7	0

In this section, we build on the results by Richter et al. (2012), and assess the thermosteric, halosteric and steric contributions to the seasonal cycle of the sea-level at each hydrographic station along the Norwegian coast.

We find that using the tide gauge data, instead of satellite altimetry measurements, only little affects the estimate of the thermosteric, halosteric and steric contributions to the seasonal cycle of SLA (Fig. 12), even though the tide gauges are not colocated in space with the hydrographic stations. Indeed, the seasonal cycle returned by satellite altimetry at each hydrographic station strongly resembles that returned by the nearby tide gauge (Fig. 12, fourth column). At the same time,

the RMSD between the seasonal cycle of the SLA and steric sea-level, scaled by the range (maximum minus minimum) of the seasonal cycle of SLA, little depends on the dataset used (Table 1, first and second columns).

We also note that density changes contribute substantially to the seasonal cycle of SLA along the Norwegian coast, as shown by Fig. 12 and Table 1. The seasonal cycle of SLA and steric sea level are 1-month out-of-phase along the southern and western coast of Norway up to Yndre-Utsira, and in-phase over the remaining part of the Norwegian coast. Moreover, the ratio between the range of seasonal cycles of steric sea-level and of SLA varies between 0.6, at Ytre Utsira, and 0.9, at Bud (Table 1, third column).

Along the Norwegian coast, the seasonal cycle of steric sea-level is more affected by variations in temperature than in salinity. We note that, with the exception of Bud and Skrova, the seasonal cycle of the steric component mostly resembles that of the thermosteric component in terms of both amplitude and phase. At the same time, we note a clear discrepancy between the seasonal cycle of the halosteric and steric components both in southern Norway, where they are in anti-phase, and at Bud, where the seasonal cycle of the halosteric sea-level is dominated by the semi-annual cycle. A more quantitative analysis returns comparable results; the RMSD between the steric and halosteric seasonal cycles exceeds by a factor of 1.4 the RMSD between the steric and thermosteric seasonal cycles along the entire coast of Norway (with the exception of Skrova, where the ratio between the two RMSDs is 0.7).

5.3.4 Detrended and deseasoned coastal sea-level and its components

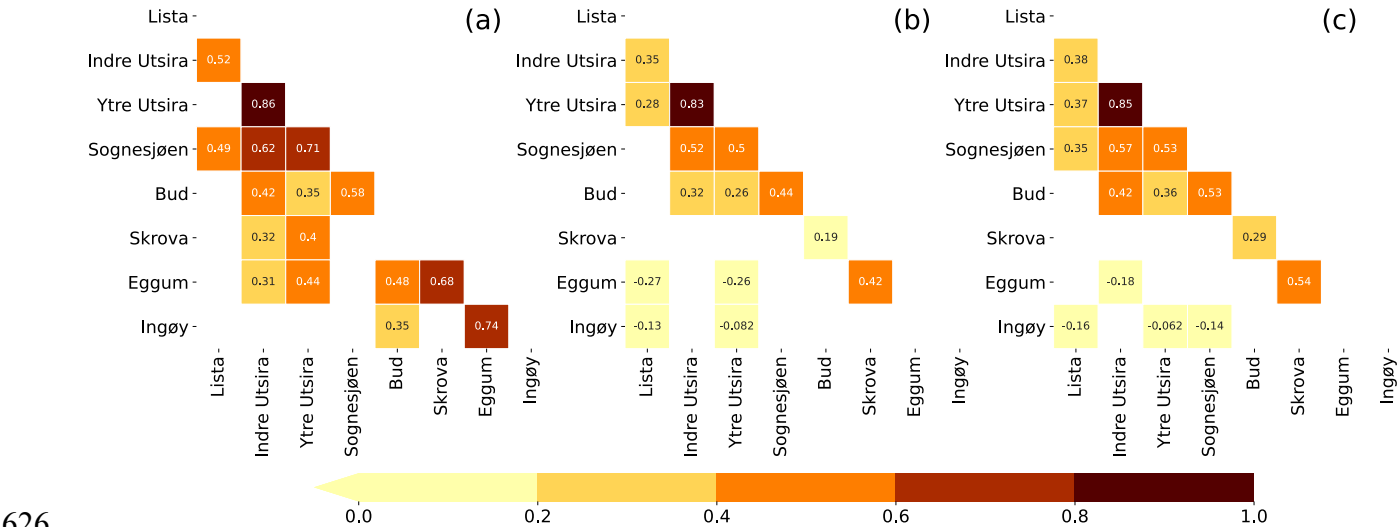


Figure 13: Correlation matrices of the detrended and deseasoned thermosteric (a), halosteric (b) and steric (c) components of the sea-level at each hydrographic station. Correlation values that are not significant at a 0.05 significance level have been omitted.

630 The detrended and deseasoned thermosteric sea-level along the Norwegian coast shows a larger spatial variability compared
631 to the detrended and deseasoned halosteric component (Fig. 13). The correlation matrix of the thermosteric sea-level (Fig.
632 13a) shows larger values compared to the one obtained considering the halosteric sea-level signals (Fig. 13b). As an
633 example, while the minimum linear correlation coefficient between two adjacent hydrographic stations in Fig. 13a is 0.49
634 0.52, it is only 0.18 0.19 in Fig. 13b. We briefly discuss the small spatial scale variability of the halosteric sea-level
635 component along the Norwegian coast in the Discussion and conclusions section of the paper.

636
637 From Fig. 13c, we also note that the values of the correlation matrix of the steric sea-level fall in between those of the
638 thermosteric and of the halosteric components. This suggests that the thermosteric and halosteric components of the sea-level
639 give a similar contribution to the sea-level variability along the Norwegian coast.

640

641 6 Discussion and conclusions

642 In this paper, we have first assessed the ability of the ALES-reprocessed satellite altimetry dataset to capture the Norwegian
643 sea-level variability over a range of timescales. Then, we have used data from hydrographic stations to quantify the steric
644 contributions and partition to the sea-level variability along the coast of Norway.

645

646 ~~When compared to conventional altimetry (Breili et al., 2017), the ALES-reprocessed altimetry dataset provides estimates of~~
647 ~~the sea-level trend along the coast of Norway that better agree with those from tide gauges. Unfortunately, we cannot~~
648 ~~directly compare the linear trends in this work with those in Breili et al. (2017) since they focus on a different period and, the~~
649 ~~sea-level trend along the Norwegian coast strongly depends on the length of the time-window considered (Fig. 9). When~~
650 ~~comparing those altimetry datasets with tide-gauge records in terms of linear trend computed over a common time window,~~
651 ~~ALES shows an improvement over the conventional open ocean retracker. This is particularly evident in northern Norway,~~
652 ~~between Bodo and Tromsø, where the difference between the linear trend from ALES and the tide gauges are small (up to~~
653 ~~0.7 mm year⁻¹), compared to circa 1 to 3 mm year⁻¹ obtained using a conventional altimetry dataset.~~

654

655 Along the Norwegian coast, the sea-level trend from the ALES-reprocessed satellite altimetry dataset is found to be
656 compatible with the estimates from tide-gauges. Their difference only ranges between -0.85 and 1.15 mm year⁻¹ and is
657 significantly different from zero at the 95% confidence level at 19 out of 22 tide gauge locations. Because of this good
658 agreement, the choice of the sea-level dataset (either tide gauges or ALES) has minimal impact on the estimates of the
659 thermosteric, of the halosteric and of the steric relative contributions to the sea-level trend. Despite the large uncertainties,
660 this result is encouraging since it suggests that the ALES dataset can be used to partition the sea-level variability in regions

661 of the coastal ocean not covered by tide gauges. At the same time, it confirms the validity of previous sea-level studies in the
662 region which only used tide gauge data (e.g., Richter et al., 2012).

663

664 Regarding the comparison between the ALES-retracked and the along-track (L3) conventional altimetry datasets, we find
665 that the former shows, on average, a 10% improvement, despite it being well within the margins of error. This improvement
666 is most evident at Bodø, Kabelvåg and Tromsø, in northern Norway, where the agreement with the tide gauges improved by
667 19%, 23% and 24% respectively. The use of the ALES retracker to more satellite altimetry missions, in order to have more
668 observations and to cover the period before July 2002, might help to reduce the uncertainties and return a more statistically
669 significant result.

670

671 A comparison with Breili et al. (2017), where an along-track (L3), multi-mission conventional altimetry dataset was used to
672 analyse the sea-level trend along the Norwegian coast, returns comparable results. We cannot, however, directly compare the
673 linear trends in this work with those in Breili et al. (2017) since they focus on a different period (1993-2016), and the sea-
674 level trend along the Norwegian coast strongly depends on the length of the time-window considered (Fig. 9). However,
675 when assessing how the conventional satellite altimetry datasets compare with tide-gauge records in terms of linear trend
676 computed over a common time-window, ALES shows again an improvement in northern Norway, between Bodø and
677 Tromsø, where the difference between the linear trend from ALES and the tide gauges are small (up to 0.5 mm year⁻¹),
678 compared to circa 1 to 3 mm year⁻¹ found by Breili et al. (2017) using a conventional altimetry dataset.

679

680 The results obtained from the ALES dataset also suggest that along the north-western coast of Norway, between Ålesund and
681 Bodø, the accuracy of remote sensed sea level records might depend on the distance from the coast. Indeed, the agreement
682 between the sea level trends estimated from satellite altimetry and the tide gauges increases as we restrict the altimetry
683 observations to 5 km from the coast. Previous studies (e.g., Marti et al., 2019; Gouzenes et al., 2020) have also reported
684 changes in the sea level trend within a few kilometres in several regions of the globe and they have argued for their physical
685 origin. The contribution of winds, river runoff and wave forcing are reported to explain the departure of the sea level trend
686 along the coast from that in the open ocean. However, while previous studies have mostly observed a sea level trend increase
687 towards the coast, our results suggest the opposite. Unfortunately, in this study, we cannot use the in-situ data to understand
688 this feature. Indeed, Bud is the only hydrographic station in the region and, due to its numerous gaps, it does not allow for a
689 clear quantification of the thermosteric and halosteric contributions to the sea level trend. A dedicated study that uses both a
690 20 Hz coastal altimetry dataset and a high resolution ocean reanalysis, such as NorShelf (Röhrs et al., 2018), could help
691 better understand whether the sea level trend actually decreases towards the coast and why.

692

693 The ALES-retracked satellite altimetry dataset is found to underestimate the amplitude of the annual cycle along large
694 portions of the Norwegian coast (Fig. 6). Even though the difference between the two sets of estimates is not significant at a
695 95% significance level (the 95% confidence interval is approximately twice the standard error), we find this result interesting
696 because of its consistency. We do not expect such a consistency to depend on the ALES retracker since we find a
697 comparable result when we use the along-track (L3) conventional altimetry product (Fig. C3). We rather suspect a
698 dependence of the amplitude of the annual cycle on the bathymetry and, therefore, on the distance from the coast, as shown
699 by Passaro et al. (2015) along the Norwegian sector of the Skagerrak.

700

701 ~~Even though the ALES altimetry dataset tend to underestimate and overestimates the amplitude of the annual cycle,~~
702 ~~respectively, to the south and to the north of Kabelvåg, a~~ comparison with Volkov and Pujol (2012) shows that ~~it~~ the
703 ALES-retracked satellite altimetry better captures the sea-level annual cycle along the coast of Norway with respect to the
704 gridded sea-level altimetry products. In that study, the authors have considered six tide gauges along the Norwegian coast,
705 namely, Kristiansund, Rørvik, Andenes, Hammerfest, Honningsvåg and Vardø to assess the quality of satellite altimetry
706 maps at the northern high latitudes. Except for Andenes, we note that the ALES-reprocessed coastal altimetry dataset allows
707 for more accurate estimates of the sea-level annual cycle, reducing the differences with the in situ sea-level records by a
708 factor of 3 to 6 compared to gridded satellite altimetry products.

709

710 We also assess the steric contribution to the seasonal cycle of SLA. Our results show that the steric variations and, in
711 particular, the thermosteric variations contribute considerably to the seasonal cycle of the sea-level along the entire
712 Norwegian coast. Moreover, we find that the relative contributions of the thermosteric, halosteric and steric sea-level little
713 depends on whether we use tide gauges or satellite altimetry. This is indicative of the large-scale spatial pattern associated
714 with the seasonal cycle of SLA.

715

716 A sea level budget analysis, performed at each hydrographic station, shows that the halosteric component of sea level
717 variability strongly influences the spatial variability of the sea level annual cycle along the Norwegian coast. Indeed, while
718 the thermosteric component peaks in October along the entire coast of Norway, the halosteric component peaks at the
719 beginning of the year in southern Norway, between October and November at Sognesjøen, and in December from the middle
720 to the north of Norway. When we compute the same analysis, but considering halosteric sea level signals over different
721 depth ranges (Fig. 14), we note that the spatial variability of the halosteric component of the sea level results from surface
722 processes: while the annual cycle of the halosteric signal at the surface has a maximum in June in southern Norway, it peaks
723 later in the year as one moves northward. The result for southern Norway agrees with Janssen et al. (1999) and Hordoir et al.
724 (2013) who show that surface salinity has a minimum in June because of the combined effect of river runoff and the

725 ~~freshwater flux from the Baltic Sea. Instead, the result for northern Norway might follow from the advection of the~~
726 ~~freshwater from the Baltic which needs a few months to reach northern Norway (Koszalka et al., 2013).~~
727

728 The detrended and deseasoned sea-level variability along the Norwegian shelf resembles the along-slope wind index proposed
729 by Chafik et al. (2019). We note that the similarities between the two are stronger along the western and the northern coast of
730 Norway than in the south. Indeed, from Oslo to Ålesund, those SLA signals depart from the along-slope winds index
731 between 2003 and 2008, probably due to local effects, such as the Baltic outflow. We refer to local effects since Chafik et al.
732 (2019) attributed the interannual sea level variability over the northern European continental shelf to the along-slope winds,
733 which might regulate the exchange of water between the open ocean and the shelf through Ekman transport.

734

735 Because the detrended and deseasoned SLA pattern is coherent over large distances along the Norwegian coast (see also
736 Chafik et al., 2017), coastal altimetry observations located a few hundred kilometres apart can be representative of the sea
737 level variations occurring at a particular tide gauge location. This explains why we can average the SLA from altimetry over
738 an area a few thousands of kilometres wide around each tide gauge location to maximize the linear correlation coefficient
739 between the detrended and deseasoned SLA from satellite altimetry and the tide gauges (Section 3.2). Moreover, it also
740 partly explains the good agreement between satellite altimetry and tide gauges since, as we average over a large number of
741 satellite altimetry observations, we reduce the noise in the SLA from altimetry which might result, for example, from the
742 rough topography of Norway.

743

744 The small-scale variability of the detrended and deseasoned sea-level halosteric component (Fig. 13) does not reconcile with
745 the good agreement between tide gauge sea-level signals and the ALES-reprocessed altimetry dataset. Indeed, to compare
746 the two datasets, we have averaged the satellite altimetry observations over an area a few hundreds of kilometres wide
747 around each tide gauge. However, Figure 13 suggests that the estimates of the halosteric component can change significantly
748 over an area of this size. Furthermore, while this component has a magnitude comparable to that of the detrended,
749 deseasoned SLA (not shown), it only explains a small fraction (from 3 to 11 %) of the difference between the sea-level
750 signals from altimetry and the tide gauges.

751

752 Future work is thus warranted to understand whether the small-scale variability of the halosteric component of the sea-level
753 along the Norwegian coast results from measurement issues. For example, ocean salinity is measured approximately once a
754 week at Skrova and approximately twice a month at the remaining hydrographic stations: this aliases the sub-weekly salinity
755 variations into the lower frequency components and, consequently, might significantly alter the monthly mean salinity
756 values. A new study, which takes benefit from ships of opportunity, synergies between different observational platforms and
757 ocean models, could help clarify this issue.

758
759
760
761
762
763
764
765
766
767
768
769
770
771
772
773
774
775
776
777
778
779
780
781
782
783
784
785
786
787

To conclude, we have demonstrated the advantage of the ALES-retracker over the conventional open ocean retracker along the coast of Norway. The retracking of earlier altimeter missions would, however, be necessary to provide a more accurate estimate of the sea level variability along the coast of Norway and possibly used to understand whether the sea-level in the region is accelerating. Still, this paper gives confidence that the ALES-reprocessed altimetry dataset can be fruitfully used to measure coastal sea level variations in regions poorly covered by tide gauges.

Appendix A

To estimate the uncertainty associated with the sea level trends derived from tide gauges and the ALES-retracked satellite altimetry dataset (Fig. 8), we need to account for the effective degrees of freedom in the sea-level anomaly time series. Indeed, successive points in the SLA time series might be correlated and, therefore, not drawn from a random sample.

To determine the effective number of degrees of freedom, we produce the variograms of the detrended and deseasoned SLA from the tide gauges and the altimetry dataset. The variogram is defined as:

$$\gamma(t) = \frac{1}{2} \cdot \text{var}[x(t) - x(t + \tau)]$$

where $x(t)$ is the time series under study, var stands for variance, and τ is the time lag.

The number of degrees of freedom is obtained by fitting the variograms with a spherical function of the form:

$$\begin{cases} c(h) = b + C_0 \cdot \left(1 - \frac{3|h|}{2a} + \frac{1|h|^3}{2a^3}\right) & \text{if } h \leq a \\ c(h) = b + C_0 & \text{if } h > a \end{cases}$$

where h is the fitting parameter, and a is the effective range or, in other words, the lag needed for the variogram to reach a constant value. Variograms are preferred to autocorrelations in geostatistics because they better detect the nonstationarity of time series.

We use the fit to determine the lag at which each variogram reaches a plateau, since it indicates the decorrelation timescale of the time series. The effective number of degrees of freedom corresponds to the ratio between the length of the time series and the lag.

788 We find that the lag only little depends on the tide gauge location, and on whether we consider the detrended and deseasoned
789 SLA from the altimetry dataset or the tide gauges (Figs. A1 and A2). The variograms obtained from both altimetry and the
790 tide gauges return a lag of 2 months at each tide gauge location, with the exception of three stations in southern Norway
791 (Viker, Oscarborg and Helgeroa), where the SLA from the tide gauges is characterized by a 3-month lag.

792

793 We use the same approach to compute the uncertainty associated with the linear trend of the difference between the SLA
794 from satellite altimetry and the tide gauges, with only one exception. We noticed that the spheric model does not fit the
795 variogram for Trondheim. Therefore, for Trondheim, we opted for an exponential model:

796

$$797 \quad \gamma(t) = b + C_0 \left(1 - e^{-\frac{h}{a}} \right)$$

798

799 where h the fitting parameter, and a is the range parameter. An exponential function is preferred over the spherical function
800 when the time series shows a strong temporal correlation.

801

802 The serial correlation is negligible along the entire Norwegian coast with the exception of Viker, Oscarborg, Oslo and
803 Narvik, where the variograms return a 2-month lag (Fig. A3). At Trondheim, instead, we find a much larger lag
804 (approximately 10 months).

805

806 We use the effective number of degrees of freedom when we compute the confidence intervals of the sea-level rates in Fig.
807 8. We compute the 95% confidence interval of the linear trend as follows:

808

$$809 \quad CI = t_{0.05/2, N^*-6} \cdot \sqrt{\frac{N-1}{N^*-1}} \cdot SE$$

810

811 where SE is the standard error of the linear trend, computed as if $N^* = N$, the total number of observations in the time series,
812 and $t_{0.05/2, N^*-6}$ is the t-values computed using $N^* - 6$ degrees of freedom at a 0.05 significance level.

813

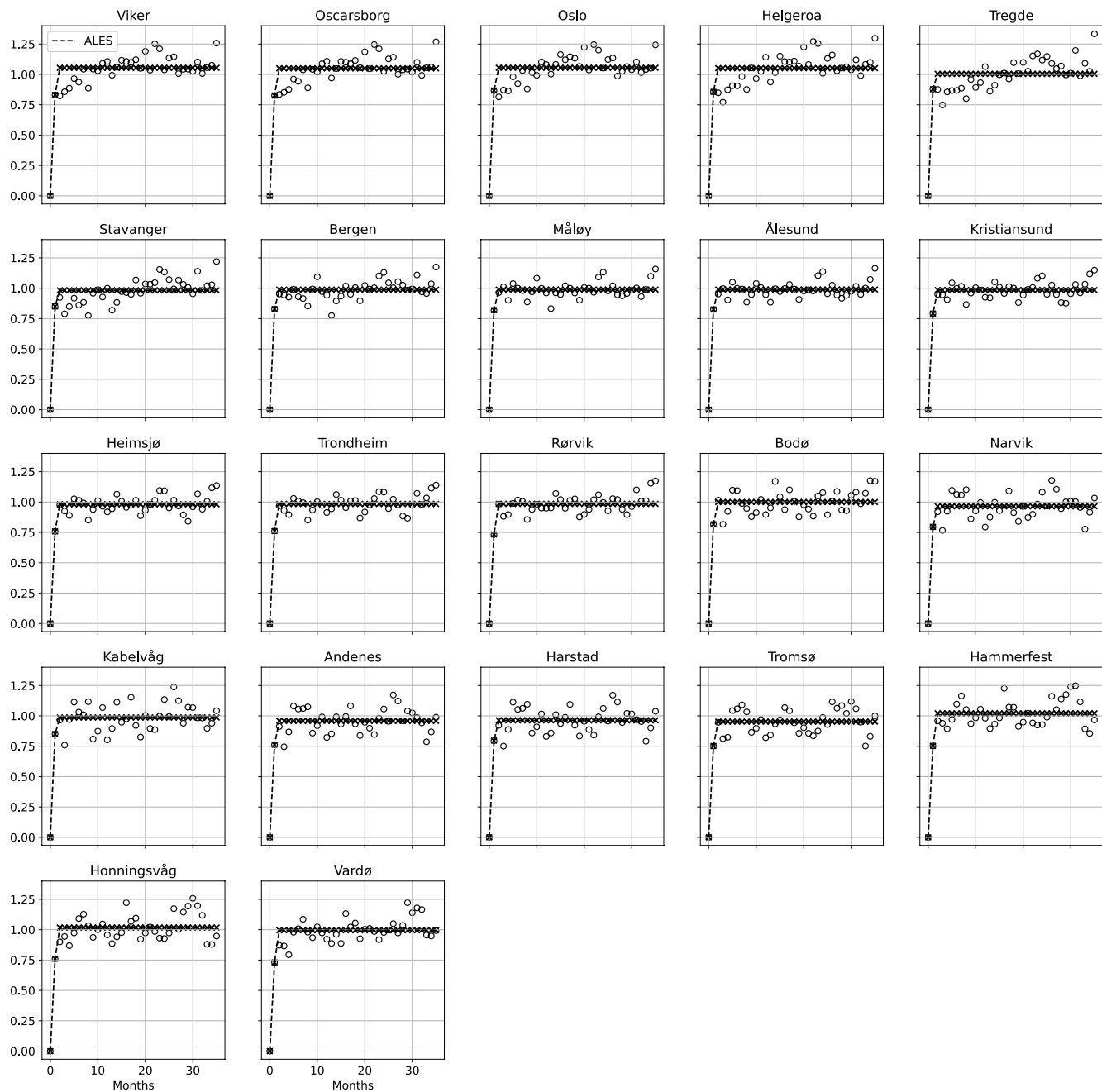
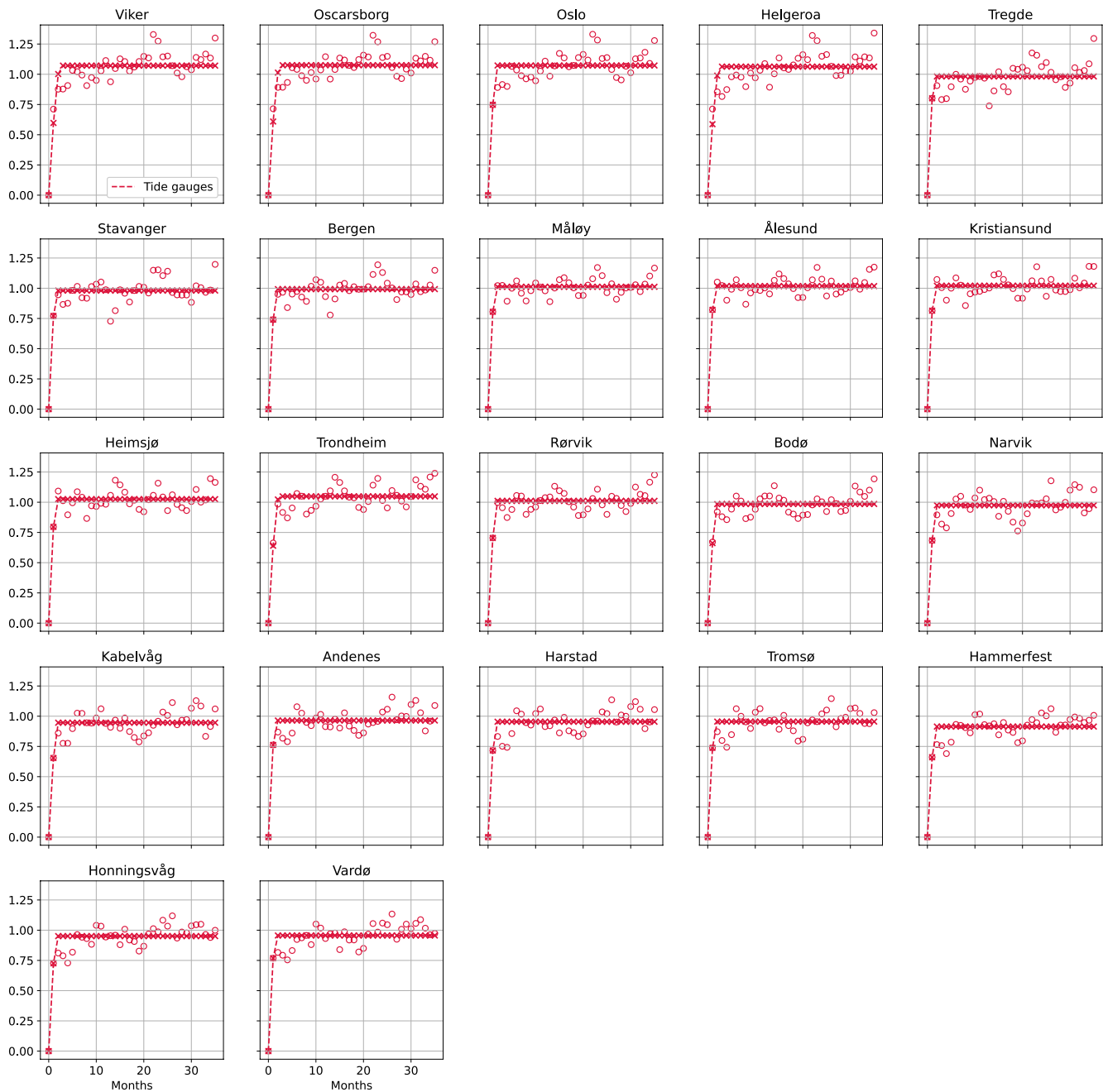


Figure A1: For each tide gauge along the Norwegian coast, variogram of the difference between the detrended and deseasoned SLA estimated from the ALES-retracker satellite altimetry (empty circles) and corresponding fit (crosses connected by a dashed line). At each tide gauge location, we scaled each variogram by the variance of the corresponding detrended and deseasoned SLA for all the plots to have the same limits on the y axis.



822

823

824

825

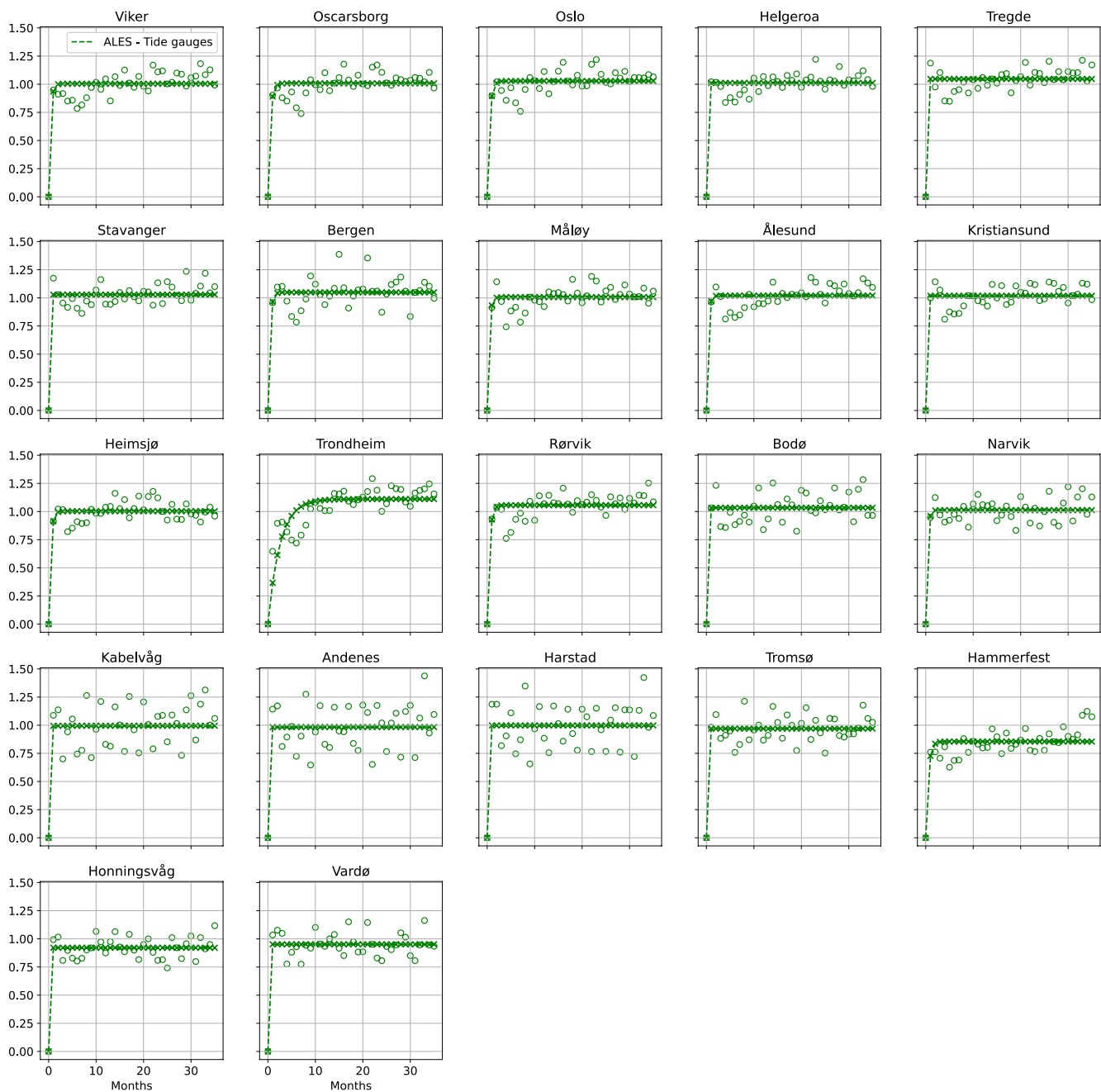
826

827

Figure A2: For each tide gauge along the Norwegian coast, variogram of the difference between the detrended and deseasoned SLA measured by the tide gauge (empty circles) and corresponding fit (crosses connected by a dashed line). At each tide gauge location, we scaled each variogram by the variance of the corresponding detrended and deseasoned SLA for all the plots to have the same limits on the y axis.

828

829



830

831

832

Figure A3: For each tide gauge along the Norwegian coast, variogram of the difference between the detrended and deseasoned SLA estimated from the ALES-retracker satellite altimetry and the tide gauge (empty circles) and corresponding fit (crosses)

connected by a dashed line). At each tide gauge location, we scaled each variogram by the variance of the corresponding detrended and deseasoned SLA for all the plots to have the same limits on the y axis.

Appendix B

Following the same argument as in the Appendix A of the Supplementary Material, to estimate the uncertainty associated with the linear trends of the thermosteric, of the halosteric and of the steric components of the sea-level along the Norwegian coast (Fig. 11), we need to account for the effective degrees of freedom in the corresponding time series.

As in Section A of the Supplementary Material, to determine the effective number of degrees of freedom, we first produce the variograms of the detrended and deseasoned thermosteric, of the halosteric and of the steric components of the sea-level at each hydrographic station. Then, we determine the time needed by the variogram's fit to approximately reach a plateau, adopting an exponential function (See Appendix A).

The thermosteric sea-level (Fig. B1) shows the strongest serial correlation. The variogram of the thermosteric sea-level returns lags ranging from 3 months, at Indre Utsira, to around 20 months at Skrova. In general, the thermosteric component of the sea-level in northern Norway has fewer degrees of freedom than in the south.

The halosteric (Fig. B2) and the steric (Fig B3) components show a similar pattern, with the number of effective degrees of freedom being smaller in the north than in the south. However, both components show a weaker serial correlation when compared to the thermosteric component of the sea-level. Indeed, the variograms return lags between 3 and 9 months for both components of the sea-level.

Similarly to the Appendix A, we use the following formula to compute the 95% confidence interval of the linear trend of the SLA and of the thermosteric, halosteric and steric components of the sea-level at each hydrographic station:

$$CI = t_{0.05/2, N^*-2} \cdot \sqrt{\frac{N-1}{N^*-1}} \cdot SE$$

where SE is the standard error of the linear trend, computed as if $N^* = N$, the total number of observations in the time series, and $t_{0.05/2, N^*-2}$ is the t-values computed using $N^* - 2$ degrees of freedom at a 0.05 significance level.

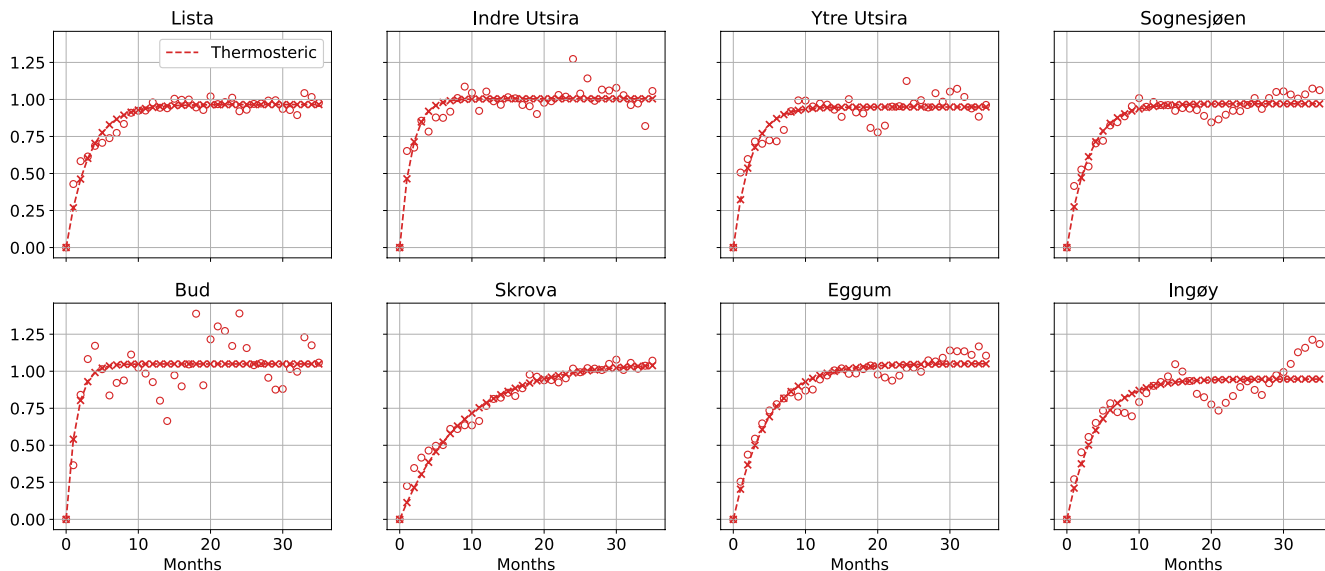


Figure B1: For each hydrographic station along the Norwegian coast, variogram of the detrended and deseasoned thermosteric component of the sea-level variability (empty circles) and corresponding fit (crosses connected by a dashed line). At each hydrographic station location, we scaled each variogram by the variance of the corresponding detrended and deseasoned thermosteric component of the sea-level for all the plots to have the same limits on the y axis.

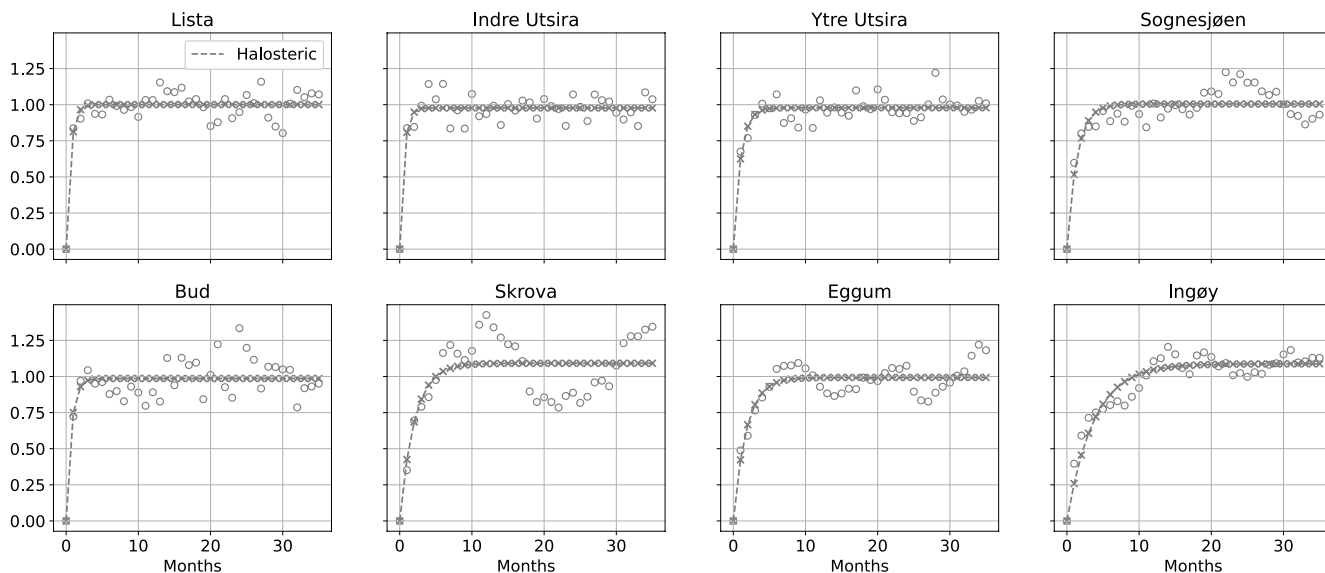
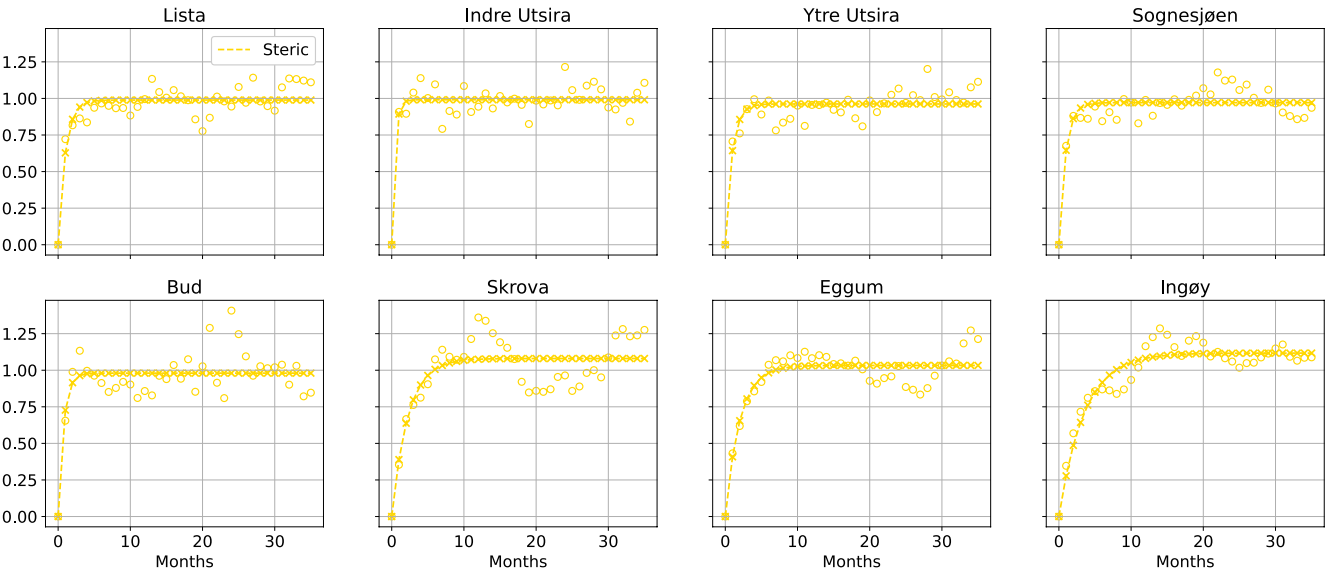


Figure B2: For each hydrographic station along the Norwegian coast, variogram of the detrended and deseasoned halosteric component of the sea-level variability (empty circles) and corresponding fit (crosses connected by a dashed line). At each

876 hydrographic station location, we scaled each variogram by the variance of the corresponding detrended and deseasoned
877 halosteric component of the sea-level for all the plots to have the same limits on the y axis.
878
879

880



881

882 **Figure B3:** For each hydrographic station along the Norwegian coast, variogram of the detrended and deseasoned steric
883 component of the sea-level variability (empty circles) and corresponding fit (crosses connected by a dashed line). At each
884 hydrographic station location, we scaled each variogram by the variance of the corresponding detrended and deseasoned steric
885 component of the sea-level for all the plots to have the same limits on the y axis.
886
887

888 Appendix C

889

890 To compare the performance of the ALES-retracked and the conventional satellite altimetry dataset, we download the along-
891 track L3 satellite altimetry missions provided on the Copernicus website: [https://resources.marine.copernicus.eu/product-
892 download/SEALEVEL_GLO_PHY_L3_REP_OBSERVATIONS_008_062](https://resources.marine.copernicus.eu/product-download/SEALEVEL_GLO_PHY_L3_REP_OBSERVATIONS_008_062).
893

893

894 We select the same satellite altimetry missions that have been reprocessed with the ALES-retracker. Moreover, we make
895 sure that both satellite altimetry datasets cover the same period.

1 - Viker	4 - Helgeroa	7 - Bergen	10 - Kristiansund	13 - Rørvik	16 - Kabelvåg	19 - Tromsø	21 - Honningsvåg
2 - Oscarsborg	5 - Tregde	8 - Måløy	11 - Heimsjø	14 - Bodø	17 - Andenes	20 - Hammerfest	22 - Vardø
3 - Oslo	6 - Stavanger	9 - Ålesund	12 - Trondheim	15 - Narvik	18 - Harstad		

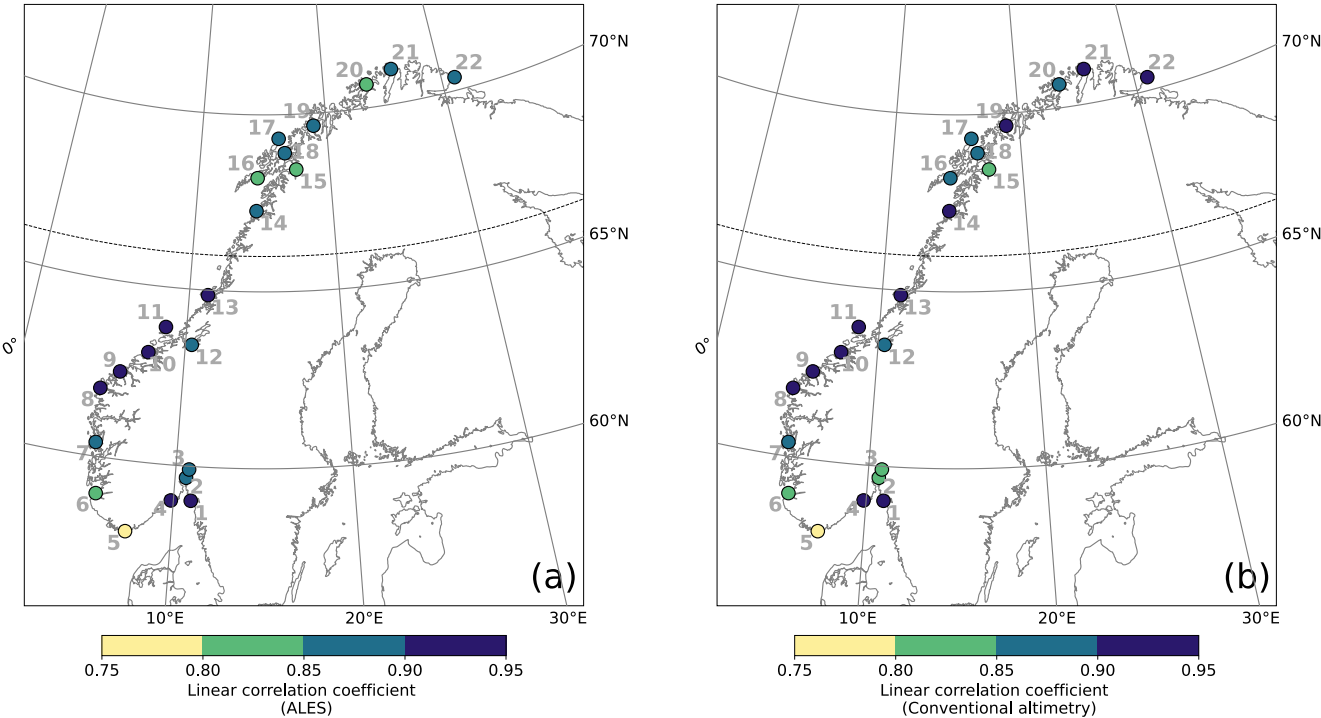


Figure C1: Comparison between coastal sea-level signals from in situ measurements and the area-averaged ALES-reprocessed satellite altimetry dataset and the conventional satellite altimetry dataset. At each tide gauge location, linear correlation coefficient between the detrended and deseasoned monthly mean SLA from the ALES-reprocessed satellite altimetry dataset and from the tide gauge (a), and from the conventional altimetry dataset and the tide gauge. The black, dashed line indicates the 66°N parallel.

1 - Viker	4 - Helgeroa	7 - Bergen	10 - Kristiansund	13 - Rørvik	16 - Kabelvåg	19 - Tromsø	21 - Honningsvåg
2 - Oscarsborg	5 - Tregde	8 - Måløy	11 - Heimsjø	14 - Bodø	17 - Andenes	20 - Hammerfest	22 - Vardø
3 - Oslo	6 - Stavanger	9 - Ålesund	12 - Trondheim	15 - Narvik	18 - Harstad		

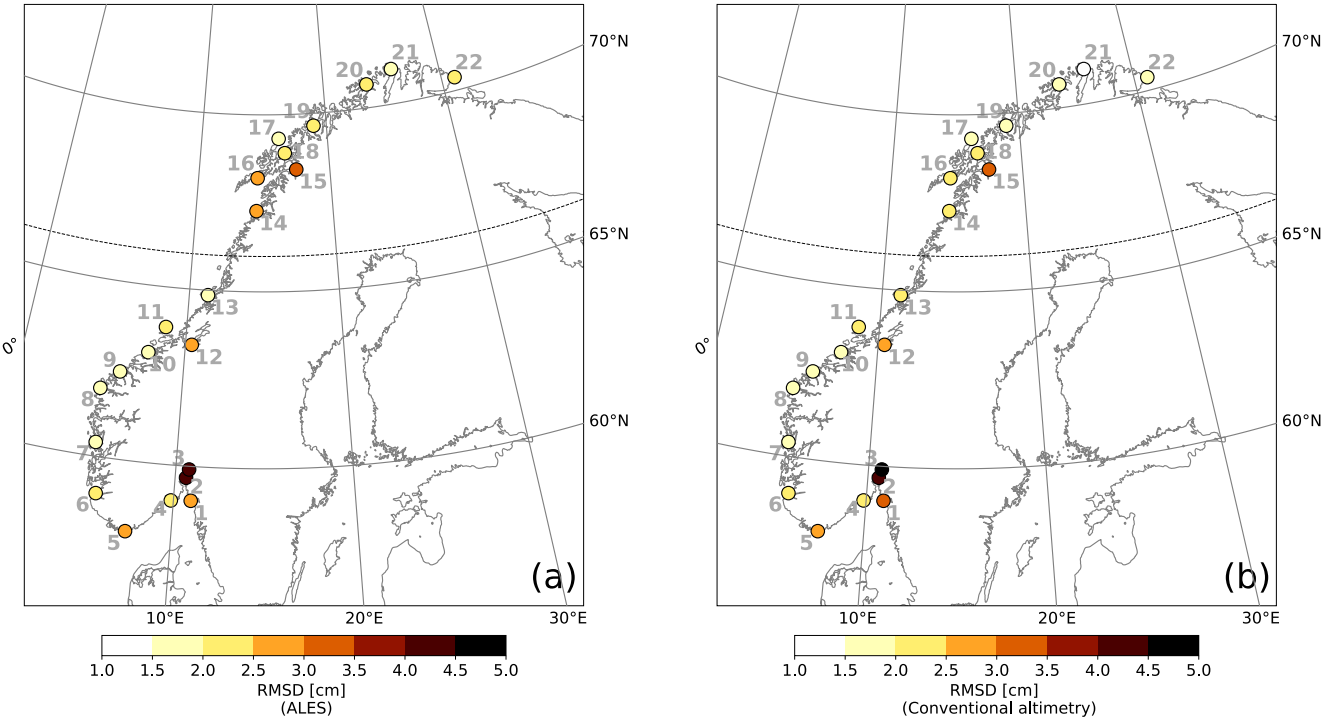


Figure C2: Comparison between coastal sea-level signals from in situ measurements and the area-averaged ALES-reprocessed satellite altimetry dataset and the conventional satellite altimetry dataset. At each tide gauge location, RMSD of the detrended and deseasoned monthly mean SLA from the ALES-reprocessed satellite altimetry dataset and from the tide gauge (a), and from the conventional altimetry dataset and the tide gauge. The black, dashed line indicates the 66°N parallel.

1 - Viker	4 - Helgeroa	7 - Bergen	10 - Kristiansund	13 - Rørvik	16 - Kabelvåg	19 - Tromsø	21 - Honningsvåg
2 - Oscarsborg	5 - Tregde	8 - Måløy	11 - Heimsjø	14 - Bodø	17 - Andenes	20 - Hammerfest	22 - Vardø
3 - Oslo	6 - Stavanger	9 - Ålesund	12 - Trondheim	15 - Narvik	18 - Harstad		

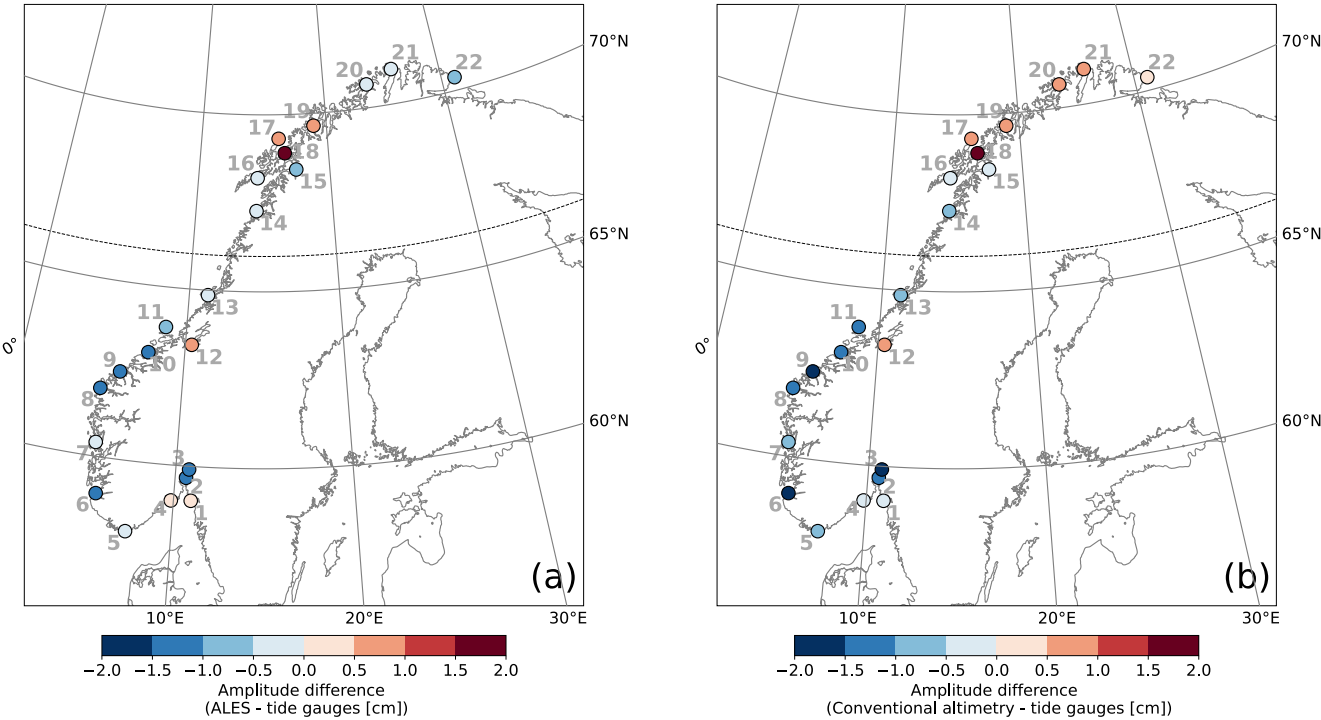


Figure C3: Comparison between coastal sea-level signals from in situ measurements and the area-averaged ALES-reprocessed satellite altimetry dataset and the conventional satellite altimetry dataset. At each tide gauge location, difference between the amplitude of the annual cycle from the ALES-reprocessed altimetry dataset and the tide gauge (a), and from the conventional altimetry dataset and the tide gauge (b). The black, dashed line indicates the 66°N parallel.

1 - Vikør	4 - Helgeroa	7 - Bergen	10 - Kristiansund	13 - Rørvik	16 - Kabelvåg	19 - Tromsø	21 - Honningsvåg
2 - Oscarsborg	5 - Tregde	8 - Måløy	11 - Heimsjø	14 - Bodø	17 - Andenes	20 - Hammerfest	22 - Vardø
3 - Oslo	6 - Stavanger	9 - Ålesund	12 - Trondheim	15 - Narvik	18 - Harstad		

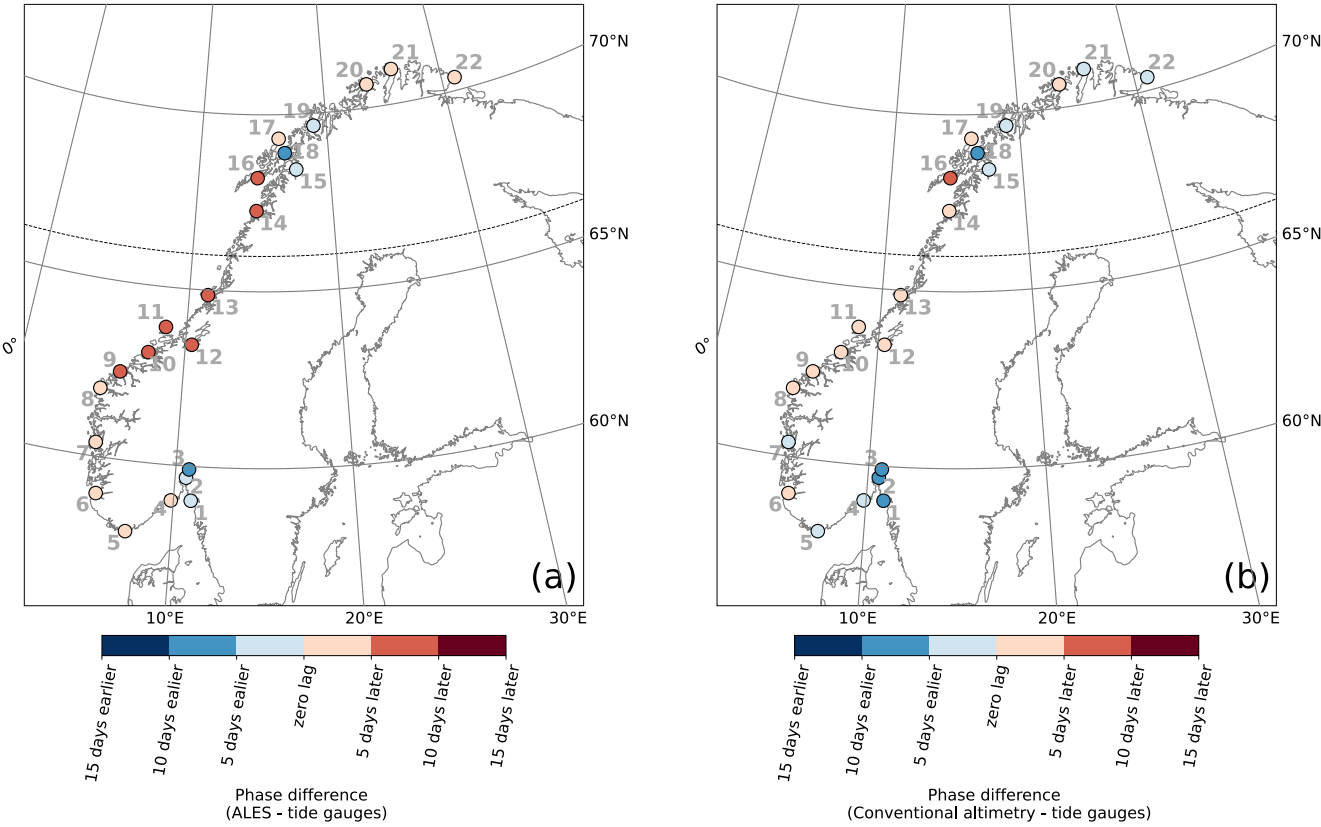


Figure C4: Comparison between coastal sea-level signals from in situ measurements and the area-averaged ALES-reprocessed satellite altimetry dataset and the conventional satellite altimetry dataset. At each tide gauge location, difference between the phase of the annual cycle from the ALES-reprocessed altimetry dataset and the tide gauge (a), and from the conventional altimetry dataset and the tide gauge (b). The black, dashed line indicates the 66°N parallel.

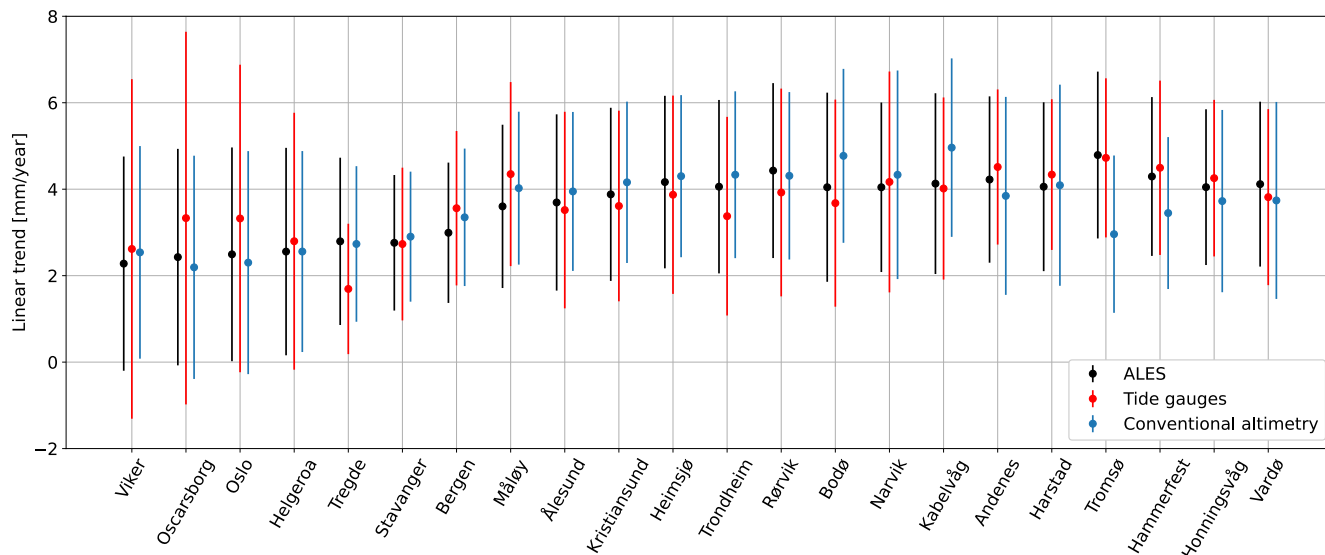


Figure C5: At each tide gauge location, linear trend of the SLA from the ALES-reprocessed altimetry dataset (black dots), from conventional altimetry dataset (cyan dots) and from tide gauges (red dots). The error bars show the 95th confidence intervals of the sea-level trend at each tide gauge location.

Data availability

The tide gauge data are available and distributed through a dedicated web API (api.schavnilva.no). The ALES-reprocessed satellite altimetry dataset is available at the Open Altimetry Database website of the Technische Universität München (<https://openadb.dgfi.tum.de/en/>). The hydrographic stations dataset are updated and available at <http://www.imr.no/forskning/forskningsdata/stasjoner/index.html>. The NCEP/NCAR v2 dataset is available at <https://psl.noaa.gov/data/gridded/data.ncep.reanalysis2.html>.

Author contribution

FM, AB, LC and LB designed the research study. JEØN removed the geophysical signal from the sea-level measured by the tide gauges. FM wrote the code to analyse the data. All authors contributed to the analysis of the results, and to the writing and the editing of the paper.

Competing interests

The authors declare that they have no conflict of interest.

Acknowledgements

947 We would like to thank the two reviewers who significantly helped improved this manuscript. All products are computed
 948 based on altimetry missions operated by NASA/CNES (TOPEX, Jason-1), ESA (ERS-1/2, Envisat, Cryosat-2),
 949 USNavy/NOAA (GFO), CNES/NASA/Eumetsat/NOAA (Jason-2, Jason-3), ISRO/CNES (SARAL), and EUMETSAT
 950 (Sentinel-3). The original data sets are disseminated by AVISO, ESA, NOAA, and PODAAC. Michael Hart-Davis (TUM) is
 951 kindly acknowledged for providing the EOT11a tidal model data. Léon Chafik acknowledges support from the Swedish
 952 National Space Agency (Dnr: 133/17, 204/19).
 953

954
 955
 956

957 References

- 958 Abulaitijiang, A., Andersen, O. B., and Stenseng, L.: Coastal sea level from inland CryoSat-2
 959 interferometric SAR altimetry, 42, <https://doi.org/10.1002/2015GL063131>, 2015.
- 960 Benveniste, J., Birol, F., Calafat, F., Cazenave, A., Dieng, H., Gouzenes, Y., Legeais, J. F., Léger, F.,
 961 Niño, F., Passaro, M., Schwatke, C., and Shaw, A.: Coastal sea level anomalies and associated trends
 962 from Jason satellite altimetry over 2002-2018, 7, 1–17, <https://doi.org/10.1038/s41597-020-00694-w>,
 963 2020.
- 964 Bonaduce, A., Pinardi, N., Oddo, P., Spada, G., and Larnicol, G.: Sea-level variability in the
 965 Mediterranean Sea from altimetry and tide gauges, 47, <https://doi.org/10.1007/s00382-016-3001-2>,
 966 2016.
- 967 Breili, K., Simpson, M. J. R., and Nilsen, J. E. Ø.: Observed sea-level changes along the Norwegian
 968 coast, 5, <https://doi.org/10.3390/jmse5030029>, 2017.
- 969 Carrère, L. and Lyard, F.: Modeling the barotropic response of the global ocean to atmospheric wind
 970 and pressure forcing - Comparisons with observations, 30, <https://doi.org/10.1029/2002GL016473>,
 971 2003.
- 972 Cazenave, A., Palanisamy, H., and Ablain, M.: Contemporary sea level changes from satellite altimetry:
 973 What have we learned? What are the new challenges?, 62, <https://doi.org/10.1016/j.asr.2018.07.017>,
 974 2018.
- 975 Chafik, L., Nilsson, J., Skagseth, and Lundberg, P.: On the flow of Atlantic water and temperature
 976 anomalies in the Nordic Seas toward the Arctic Ocean, 120, <https://doi.org/10.1002/2015JC011012>,
 977 2015.
- 978 Chafik, L., Nilsen, J. E. Ø., and Dangendorf, S.: Impact of North Atlantic teleconnection patterns on
 979 northern European sea level, 5, <https://doi.org/10.3390/jmse5030043>, 2017.
- 980 Chafik, L., Nilsen, J. E. Ø., Dangendorf, S., Reverdin, G., and Frederikse, T.: North Atlantic Ocean
 981 Circulation and Decadal Sea Level Change During the Altimetry Era, 9, <https://doi.org/10.1038/s41598-018-37603-6>, 2019.
- 982
 983 Cipollini, P., Benveniste, J., Bouffard, J., Emery, W., Fenoglio-Marc, L., Gommenginger, C., Griffin,
 984 D., Høyer, J., Kuparov, A., Madsen, K., Mercier, F., Miller, L., Pascual, A., Ravichandran, M.,
 985 Shillington, F., Snaith, H., Sturb, P. T., Vandemark, D., Vignudelli, S., Wilkin, J., Woodworth, P., and

986 Zavala-Garay, J.: The Role of Altimetry in Coastal Observing Systems,
 987 <https://doi.org/10.5270/oceanobs09.cwp.16>, 2010.

988 Cipollini, P., Benveniste, J., Birol, F., Joana Fernandes, M., Obligis, E., Passaro, M., Ted Strub, P.,
 989 Valladeau, G., Vignudelli, S., and Wilkin, J.: Satellite altimetry in coastal regions, in: Satellite
 990 Altimetry Over Oceans and Land Surfaces, <https://doi.org/10.1201/9781315151779>, 2017.

991 Frederikse, T., Jevrejeva, S., Riva, R. E. M., and Dangendorf, S.: A consistent sea-level reconstruction
 992 and its budget on basin and global scales over 1958-2014, 31, [https://doi.org/10.1175/JCLI-D-17-](https://doi.org/10.1175/JCLI-D-17-0502.1)
 993 0502.1, 2018.

994 Gill, A. E. and Niller, P. P.: The theory of the seasonal variability in the ocean, 20,
 995 [https://doi.org/10.1016/0011-7471\(73\)90049-1](https://doi.org/10.1016/0011-7471(73)90049-1), 1973.

996 Gómez-Enri, J., Vignudelli, S., Quartly, G. D., Gommenginger, C. P., Cipollini, P., Challenor, P. G.,
 997 and Benveniste, J.: Modeling Envisat RA-2 waveforms in the coastal zone: Case study of calm water
 998 contamination, 7, 474–478, <https://doi.org/10.1109/LGRS.2009.2039193>, 2010.

999 Ji, M., Reynolds, R. W., and Behringer, D. W.: Use of TOPEX/Poseidon sea level data for Ocean
 000 analyses and ENSO prediction: Some early results, 13, [https://doi.org/10.1175/1520-](https://doi.org/10.1175/1520-0442(2000)013<0216:UOTPSL>2.0.CO;2)
 001 0442(2000)013<0216:UOTPSL>2.0.CO;2, 2000.

002 Lichter, M., Vafeidis, A. T., Nicholls, R. J., and Kaiser, G.: Exploring data-related uncertainties in
 003 analyses of land area and population in the “Low-Elevation Coastal Zone” (LECZ), 27,
 004 <https://doi.org/10.2112/JCOASTRES-D-10-00072.1>, 2011.

005 Liebmann, B., Dole, R. M., Jones, C., Bladé, I., and Allured, D.: Influence of choice of time period on
 006 global surface temperature trend estimates, 91, <https://doi.org/10.1175/2010BAMS3030.1>, 2010.

007 Madsen, K. S., Høyer, J. L., Suursaar, Ü., She, J., and Knudsen, P.: Sea Level Trends and Variability of
 008 the Baltic Sea From 2D Statistical Reconstruction and Altimetry, 7,
 009 <https://doi.org/10.3389/feart.2019.00243>, 2019.

010 Nerem, R. S., Chambers, D. P., Choe, C., and Mitchum, G. T.: Estimating Mean Sea Level Change
 011 from the TOPEX and Jason Altimeter Missions, 33, <https://doi.org/10.1080/01490419.2010.491031>,
 012 2010.

013 Oppenheimer, M., Glavovic, B., Hinkel, J., van de Wal, R., Magnan, A. K., Abd-Elgawad, A., Cai, R.,
 014 Cifuentes-Jara, M., DeConto, R. M., Ghosh, T., Hay, J., Isla, F., Marzeion, B., Meyssignac, B., and
 015 Sebesvari, Z.: Sea Level Rise and Implications for Low Lying Islands, Coasts and Communities., 355,
 016 2019.

017 Passaro, M., Cipollini, P., Vignudelli, S., Quartly, G. D., and Snaith, H. M.: ALES: A multi-mission
 018 adaptive subwaveform retracker for coastal and open ocean altimetry, 145,
 019 <https://doi.org/10.1016/j.rse.2014.02.008>, 2014.

020 Passaro, M., Cipollini, P., and Benveniste, J.: Annual sea level variability of the coastal ocean: The
 021 Baltic Sea-North Sea transition zone, 120, <https://doi.org/10.1002/2014JC010510>, 2015.

022 Passaro, M., Dinardo, S., Quartly, G. D., Snaith, H. M., Benveniste, J., Cipollini, P., and Lucas, B.:
 023 Cross-calibrating ALES Envisat and CryoSat-2 Delay-Doppler: A coastal altimetry study in the
 024 Indonesian Seas, 58, <https://doi.org/10.1016/j.asr.2016.04.011>, 2016.

025 Passaro, M., Rose, S. K., Andersen, O. B., Boergens, E., Calafat, F. M., Dettmering, D., and
 026 Benveniste, J.: ALES+: Adapting a homogenous ocean retracker for satellite altimetry to sea ice leads,
 027 coastal and inland waters, 211, <https://doi.org/10.1016/j.rse.2018.02.074>, 2018.
 028 Passaro, M., Müller, F. L., Oelsmann, J., Rautiainen, L., Dettmering, D., Hart-Davis, M. G.,
 029 Abulaitijiang, A., Andersen, O. B., Høyer, J. L., Madsen, K. S., Ringgaard, I. M., Särkkä, J., Scarrott,
 030 R., Schwatke, C., Seitz, F., Tuomi, L., Restano, M., and Benveniste, J.: Absolute Baltic Sea Level
 031 Trends in the Satellite Altimetry Era: A Revisit, 8, <https://doi.org/10.3389/fmars.2021.647607>, 2021.
 032 Picaut, J., Hackert, E., Busalacchi, A. J., Murtugudde, R., and Lagerloef, G. S. E.: Mechanisms of the
 033 1997–1998 El Niño–La Niña, as inferred from space-based observations, 107,
 034 <https://doi.org/10.1029/2001jc000850>, 2002.
 035 Raj, R. P., Andersen, O. B., Johannessen, J. A., Gutknecht, B. D., Chatterjee, S., Rose, S. K., Bonaduce,
 036 A., Horwath, M., Rannal, H., Richter, K., Palanisamy, H., Ludwigsen, C. A., Bertino, L., Nilsen, J. E.
 037 Ø., Knudsen, P., Hogg, A., Cazenave, A., and Benveniste, J.: Arctic sea level budget assessment during
 038 the grace/argo time period, 12, <https://doi.org/10.3390/rs12172837>, 2020.
 039 Richter, K., Nilsen, J. E. Ø., and Drange, H.: Contributions to sea level variability along the Norwegian
 040 coast for 1960–2010, 117, <https://doi.org/10.1029/2011JC007826>, 2012.
 041 Richter, K., Meyssignac, B., Slangen, A. B. A., Melet, A., Church, J. A., Fettweis, X., Marzeion, B.,
 042 Agosta, C., Ligtenberg, S. R. M., Spada, G., Palmer, M. D., Roberts, C. D., and Champollion, N.:
 043 Detecting a forced signal in satellite-era sea-level change, 15, [https://doi.org/10.1088/1748-](https://doi.org/10.1088/1748-9326/ab986e)
 044 [9326/ab986e](https://doi.org/10.1088/1748-9326/ab986e), 2020.
 045 Rose, S. K., Andersen, O. B., Passaro, M., Ludwigsen, C. A., and Schwatke, C.: Arctic ocean sea level
 046 record from the complete radar altimetry era: 1991–2018, 11, <https://doi.org/10.3390/rs11141672>, 2019.
 047 von Schuckmann, K., le Traon, P. Y., Smith, N., Pascual, A., Brasseur, P., Fennel, K., Djavidnia, S.,
 048 Aaboe, S., Fanjul, E. A., Autret, E., Axell, L., Aznar, R., Benincasa, M., Bentamy, A., Boberg, F.,
 049 Bourdallé-Badie, R., Nardelli, B. B., Brando, V. E., Bricaud, C., Breivik, L. A., Brewin, R. J. W.,
 050 Capet, A., Ceschin, A., Ciliberti, S., Cossarini, G., de Alfonso, M., de Pascual Collar, A., de Kloe, J.,
 051 Deshayes, J., Desportes, C., Drévilion, M., Drillet, Y., Droghei, R., Dubois, C., Embury, O., Etienne,
 052 H., Fratianni, C., Lafuente, J. G., Sotillo, M. G., Garric, G., Gasparin, F., Gerin, R., Good, S., Gourrion,
 053 J., Grégoire, M., Greiner, E., Guinehut, S., Gutknecht, E., Hernandez, F., Hernandez, O., Høyer, J.,
 054 Jackson, L., Jandt, S., Josey, S., Juza, M., Kennedy, J., Kokkini, Z., Korres, G., Kōuts, M., Lagemaa, P.,
 055 Lavergne, T., le Cann, B., Legeais, J. F., Lemieux-Dudon, B., Levier, B., Lien, V., Maljutenko, I.,
 056 Manzano, F., Marcos, M., Marinova, V., Masina, S., Mauri, E., Mayer, M., Melet, A., Mélin, F.,
 057 Meyssignac, B., Monier, M., Müller, M., Mulet, S., Naranjo, C., Notarstefano, G., Paulmier, A.,
 058 Gomez, B. P., Pérez Gonzalez, I., Peneva, E., Perruche, C., Peterson, K. A., Pinardi, N., Pisano, A.,
 059 Pardo, S., Poulain, P. M., Raj, R. P., Raudsepp, U., Ravdas, M., Reid, R., Rio, M. H., Salon, S.,
 060 Samuelsen, A., Sammartino, M., et al.: Copernicus Marine Service Ocean State Report, 11,
 061 <https://doi.org/10.1080/1755876X.2018.1489208>, 2018.
 062 Siegmund, F., Johannessen, J., Drange, H., Mork, K. A., and Korabely, A.: Steric height variability in
 063 the Nordic Seas, 112, <https://doi.org/10.1029/2007JC004221>, 2007.

064 Simpson, M. J. R., Nilsen, J. E. Ø., Ravndal, O. R., Breili, K., Sande, H., Kierulf, H. P., Steffen, H.,
065 Jansen, E., Carson, M., and Vestøl, O.: Sea Level Change for Norway Past and Present Observations
066 and Projections to 2100, 1–156 pp., 2015.

067 Simpson, M. J. R., Ravndal, O. R., Sande, H., Nilsen, J. E. Ø., Kierulf, H. P., Vestøl, O., and Steffen,
068 H.: Projected 21st century sea-level changes, observed sea level extremes, and sea level allowances for
069 Norway, 5, <https://doi.org/10.3390/jmse5030036>, 2017.

070 Volkov, D. L. and Pujol, M. I.: Quality assessment of a satellite altimetry data product in the Nordic,
071 Barents, and Kara seas, 117, <https://doi.org/10.1029/2011JC007557>, 2012.

072 Woodworth, P. L.: A note on the nodal tide in sea level records, [https://doi.org/10.2112/JCOASTRES-](https://doi.org/10.2112/JCOASTRES-D-11A-00023.1)
073 [D-11A-00023.1](https://doi.org/10.2112/JCOASTRES-D-11A-00023.1), 2012.

074 Xu, X.-Y., Xu, K., Xu, Y., and Shi, L.-W.: Coastal Altimetry: A Promising Technology for the Coastal
075 Oceanography Community, in: Estuaries and Coastal Zones - Dynamics and Response to
076 Environmental Changes, 1–19, <https://doi.org/10.5772/intechopen.89373>, 2019.

077 Zhang, Z., Lu, Y., and Hsu, H.: Detecting ocean currents from satellite altimetry, satellite gravity and
078 ocean data, in: International Association of Geodesy Symposia, [https://doi.org/10.1007/978-3-540-](https://doi.org/10.1007/978-3-540-49350-1_3)
079 [49350-1_3](https://doi.org/10.1007/978-3-540-49350-1_3), 2007.

080

081
082